Irrigation - Appendix

Collection 7

General coordinator
Bernardo Rudorff

Team
Adriana Moreira
Joelen Silva
Kênia Santos
Luciana Oliveira
Moisés Salgado
Paulo Teixeira

1 Overview of the classification method

The MapBiomas project produces, among other land use and land cover classes, annual agriculture maps in Brazil from 1985 to the present. The first irrigation agriculture map from MapBiomas was released on Collection 5 together with the land use and land cover maps, in 2020. The first irrigation agriculture map consisted of mapping center pivot irrigation, covering all Brazil, and other irrigation systems, covering only the semiarid region, and both maps comprising from 2000 to 2019. In the next Collection (Collection 6), the irrigation rice class was added and the other maps, from the previous Collection, were extended to the 1985-2020 period. Currently, MapBiomas irrigation agriculture map is on third Collection, and presents a new type of information about irrigation, the pivot dynamic. Pivot dynamics consists in presenting individualized characteristics of each pivot, such as number of cycles per year, dates of start and end cycles, and average daily precipitation. Figure 1 presents the evolution of irrigation agriculture classes within the MapBiomas project.

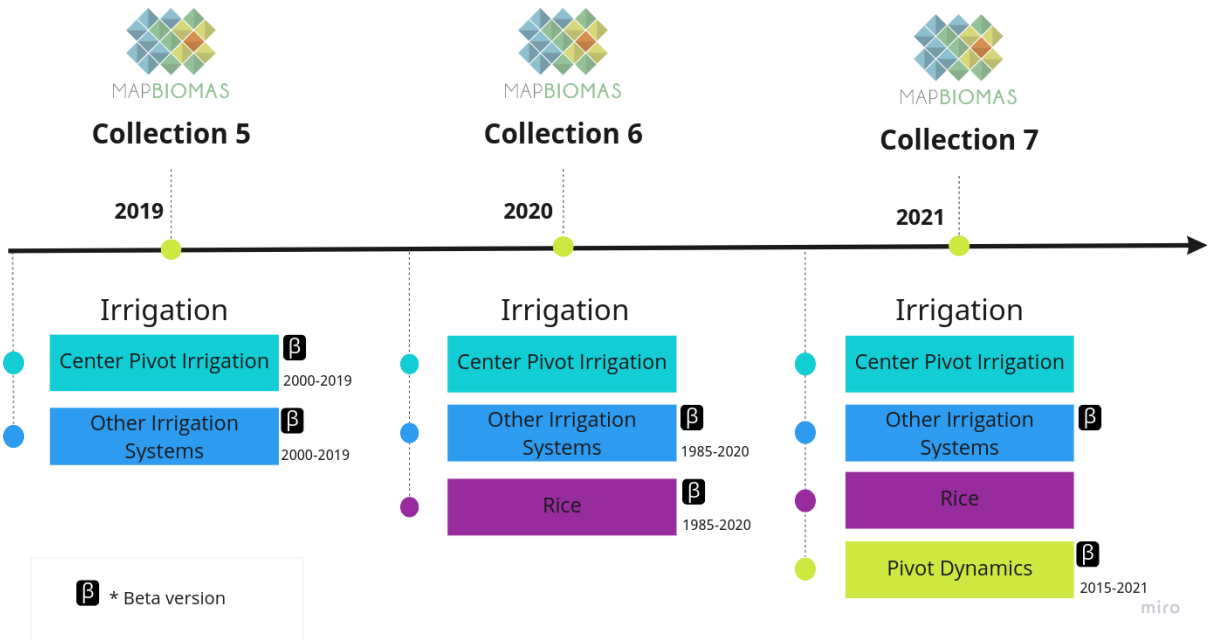

Figure 1: Comparison between the ' Irrigation Agriculture' classes of MapBiomas Collection 5, 6 and 7.

2 Center pivot irrigation systems

The first attempts in the MapBiomas project for mapping center pivot irrigation systems came through the Next Generation Mapping (NexGenMap) project. The objective of this initiative was to develop machine learning algorithms, tools and methods for producing the most current, detailed and accurate maps of land use and land cover using daily PlanetScope imagery, cloud computing, and new artificial intelligence algorithms. In the NextGenMap project, artificial intelligence algorithms were developed to map center pivot irrigation systems using PlanetScope imagery in a study area located in the Cerrado biome (SARAIVA et al., 2020). In MapBiomas context, the mapping of 'Center pivot irrigation systems'

was performed using Landsat imagery and an adapted U-Net architecture (RONNEBERGER et al., 2015), an image segmentation convolutional neural network architecture. The adapted U-Net architecture was trained with two different sets of samples, one set with center pivot irrigation systems samples and other with irrigated rice samples. To increase the temporal and spatial consistency of the final maps, the raw result was post-processed using temporal and spatial filters (Figure 2).

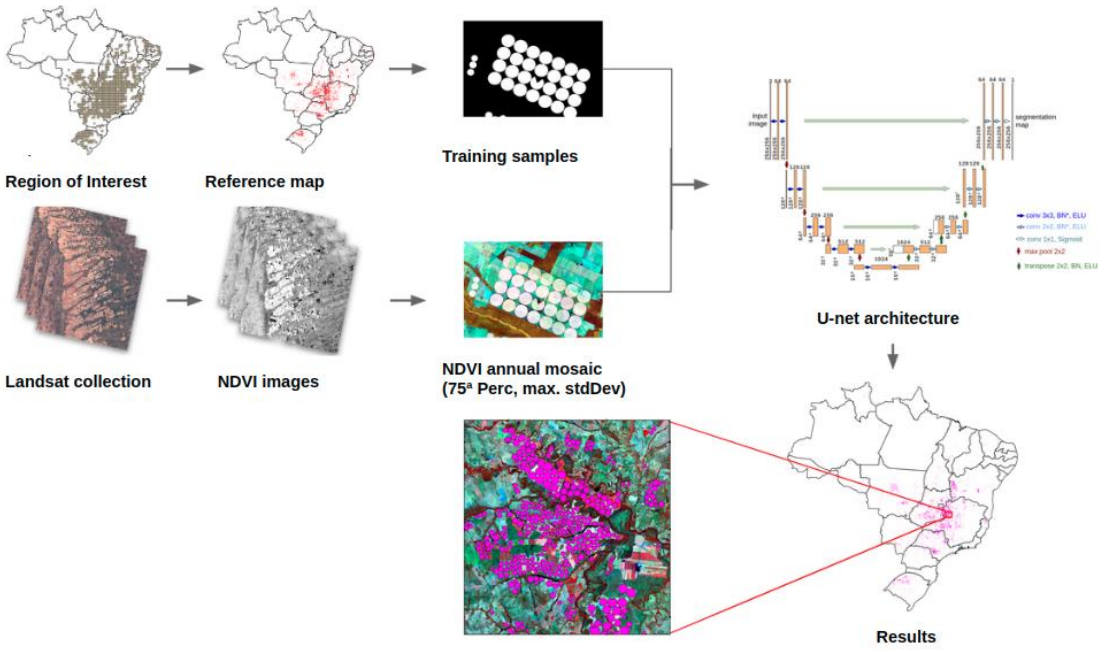

Figure 2: steps of the mapping process of two center pivot irrigation systems.

2.1 Image selection

The mapping of the center pivot irrigation systems used annual mosaics generated from available images in each year. Therefore, images from the Landsat series were obtained on the Google Earth Engine platform (Collection 1 Tier 1 TOA) in the period of 1985 to 2021. Only images with under 80% of cloud cover and shadows were considered.

2.2 Definition of regions for classification

The reference maps used to classify center pivot irrigation systems were produced by the Brazilian National Water Agency in partnership with Embrapa Milho e Sorgo, referring to the years 1985, 1990, 2000, 2005, 2010, 2014, and 2017 (ANA, 2019a). These mappings were produced using visual interpretation in images obtained by the Landsat 5, Landsat 8, and Sentinel 2A/2B satellites, as well as high-resolution images (<1 meter) from Google Earth.

For the delimitation of the study area, the Brazilian territory was divided into blocks of 0.5' x 0.5' degrees (~300 thousand ha each). Only blocks with occurrence of center pivot irrigation systems in any of the reference map years were selected. Figure 3 shows the 723 chosen blocks distributed across an area of approximately 212 million hectares to map center pivot irrigation systems in Brazil.

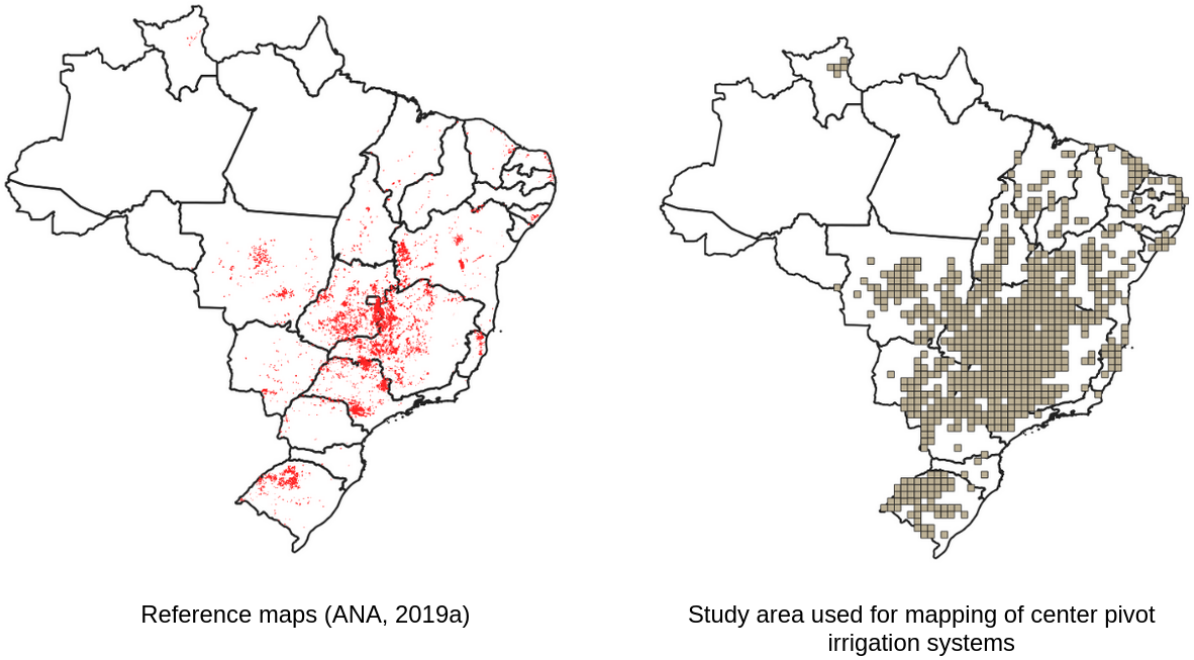

Figure 3. Study area for the mapping of center pivot irrigation systems in Brazil in the MapBiomas Collection 7.

2.3 Classification

2.3.1 Classification scheme

Each class of interest was mapped separately. Therefore, three independent classifications were performed to map: 1) Center pivot irrigation systems; 2) Irrigated rice; and 3) Other irrigation systems. The center pivot irrigation systems mapping considered only two possible classes for each pixel, center pivot irrigation systems, and non-center pivot irrigation systems.

2.3.2 Feature space

The feature space created for the center pivot irrigation systems mapping aimed to obtain the characteristics of the pivot at the time they were cultivated, as well as to highlight the differences in relation to the other targets, such as other agriculture areas, pasture, forest formation, etc. Therefore, three metrics were selected that showed the best results to distinguish the pivots in relation to the other targets:

- NDVI_p75, 75th percentile of NDVI values for all images;

- NDVI_p100, 100th percentile, or maximum value, of the NDVI values of all images, and;

- NDVI_stdDev, the standard deviation of the NDVI values for all images.

The mosaic generated is composed by the selected metrics. Each metric corresponds to a band in the image, as shown in Figure 4.

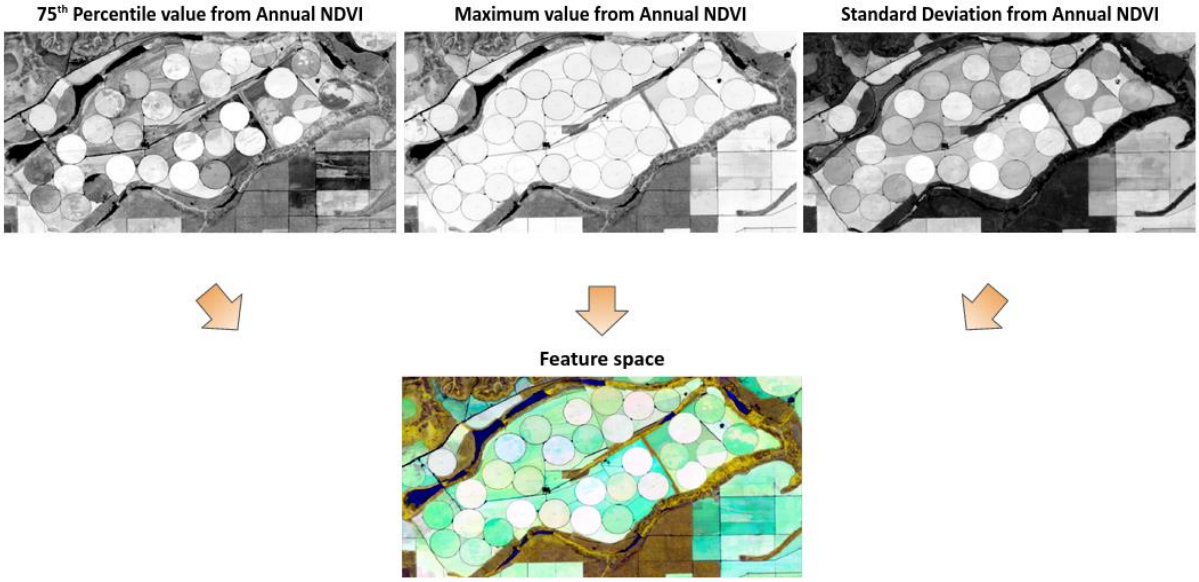

Figure 4. RGB visualization (NDVI p75, NDVI Maximum, NDVI stdDev) of an image used for training and mapping of the center pivot irrigation systems, generated for the year 2017.

The use of images with only three bands accelerated the process of training and classifying the pivots since the reduced amount of bands also reduced the computational infrastructure necessary for the processing of this data.

2.3.3 Classification algorithm, training samples and parameters

Due to the extensive study area (~212 Mha) and computational limitations, the model was trained using only a subset of blocks chosen from the population of 723 blocks. The choice of sample data is an important step for training Deep Learning models, once the samples must represent all the spatial and spectral variability of the population. For this, stratified sampling was performed based on the pivot area obtained from the reference maps. The sampling considered three strata: with low, medium and high coverage of center pivot irrigation systems. The stratum containing blocks with low coverage was created from the blocks whose pivot area was less than or equal to the median of the area of all blocks, that is, 50% of the blocks (361 blocks). The stratum with the high coverage was created from blocks whose sum of the area of its pivots covers about 50% of the pivot area of the entire population (total of 41 blocks). Finally, the remaining blocks (321 blocks) were used to create the layer with blocks containing a medium cover of center pivot irrigation systems. After creating the stratum, 20 blocks were randomly chosen for training and 10 blocks for testing in each of the three

stratum. The training blocks were used to calibrate the model, while the test blocks were used later for the accuracy analysis of the model. Figure 5 illustrates the spatial distribution of the stratum and blocks chosen for training and testing the population model.

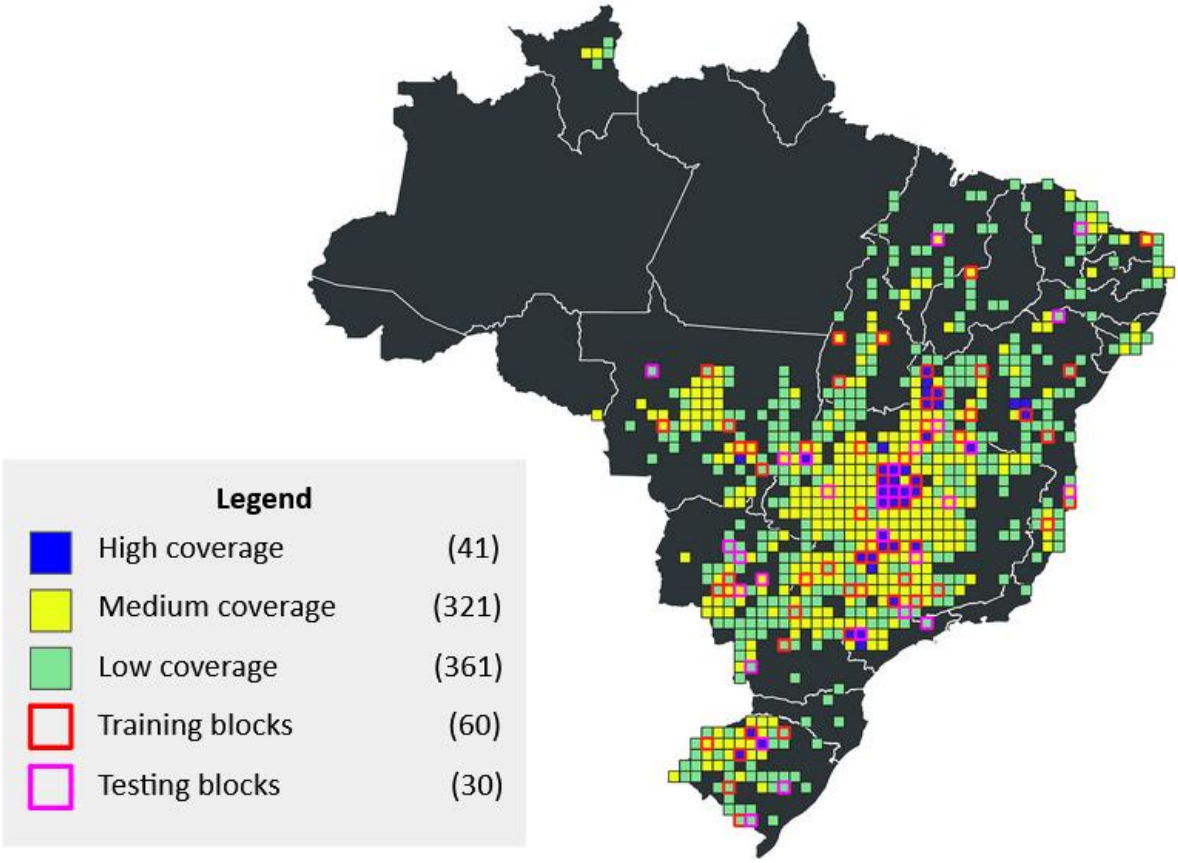

Figure 5. Spatial distribution of high, medium and low center pivot irrigation cover stratum and location of the blocks used for training and testing the model in Brazil.

As mentioned earlier, an adaptation of the U-Net convolutional neural network architecture was performed to map the center pivot irrigation systems. Figure 6 illustrates the modified U-Net architecture created.

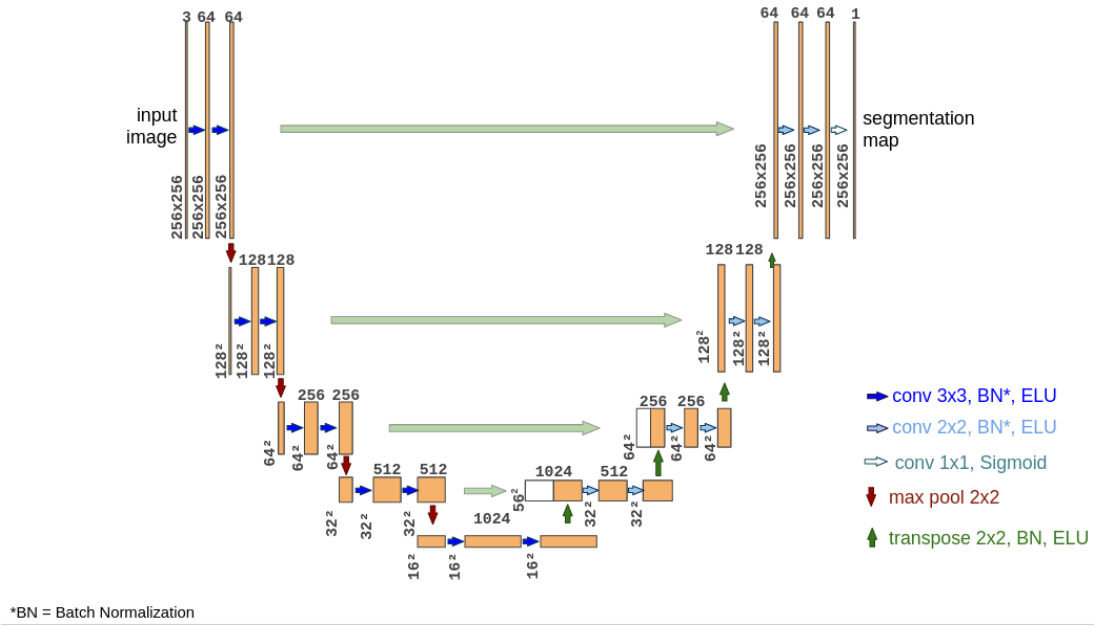

Figure 6. Adapted U-Net architecture, with its layers and connections, used for the mapping of center pivot irrigation systems.

This architecture was developed in Python, using the TensorFlow 2.0 library. The entire training and mapping process was carried out using the Google Colab platform using Google Drive to access the annual mosaics (generated in Google Earth Engine). Table 1 presents some hyperparameters used during model training.

Table 1. Hyperparameters for training the modified U-Net architecture.

Hyperparameter	Value
Chip size	256 x 256 pixels
Batch size	20
Epochs	100
Learning rate	0.001

The 2017 reference map was used for model training. In the training blocks, chips with 256 x 256 pixels were generated, 75% were allocated to the training data set and 25% for the validation data set. Figure 7 illustrates the process of subdividing training blocks into smaller chips to be used as input for model training.

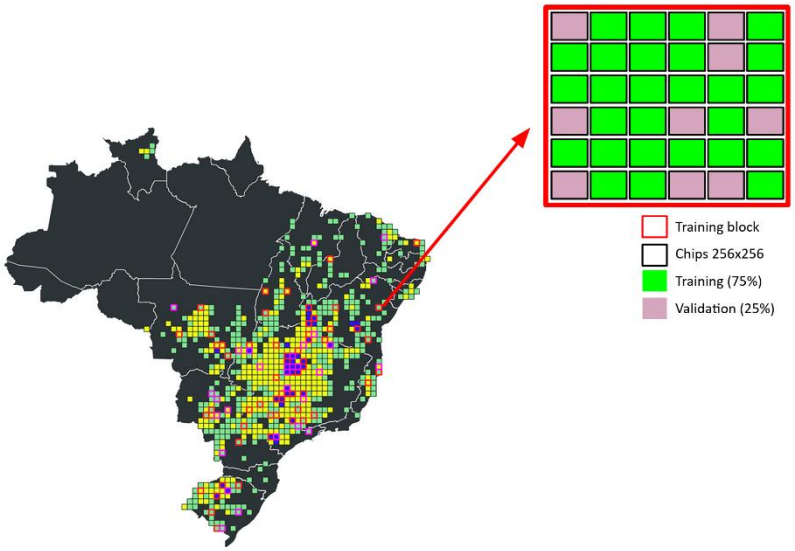

Figure 7. Examples of the training and validation chips allocated within the training block of the model.

The training set was used to learn the model and the validation set used to perform initial validations during model learning.

Once the network training process was completed, the classifier was applied throughout the Brazilian territory. In this step, 1024 x 1024 pixel chips were used. Increasing the size of the chips at the time of sorting not only decreases problems generated by the edges of the chips but also increases the memory capacity required for processing. Therefore, it was necessary to decrease the batch size to 1.

2.4 Post-Classification

2.4.1 Temporal filter

The temporal filter applied to maps of center pivot irrigation systems consisted of a five-year moving window in which the assessed pixel of the window was changed following two rules:

1. the pixel is changed to center pivot if at least one of the two previous years and at least one of the two subsequent years, that pixel was mapped as a pivot, indicating a possible model omission error;

2. pixels that were mapped as pivots only in the assessed pixel of the five-year window, indicating a possible inclusion error, have been removed from the classification.

2.4.2 Spatial filter

In the center pivot irrigation systems mapping it was used a spatial filter based on the erosion operation followed by an expansion operation using a circular kernel with a radius of

60 meters. This spatial filter helped to eliminate noise generated by the mapping, as well as smoothing the edges of the center pivot irrigation (Figure 8).

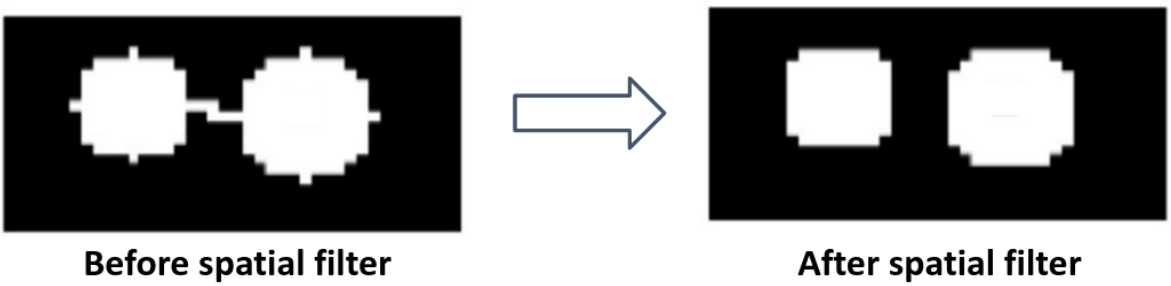

Figure 8 Example of correction of the spatial filter (on the right) in a classification that presents noise on the edges (on the left).

2.5 Validation strategies

The preliminary validation of the center pivot irrigation model used the test blocks of the 2017 mapping (see Figure 5), as these blocks were not used for the model training. From the reference map, the user's and producer's accuracy was calculated for each of the individual stratum and also considering all strata at the same time. Table 2 presents the results of the preliminary model validation.

Table 2. Preliminary validation of the center pivot irrigation mapping for the year 2017, using the test blocks selected in each stratum.

Stratum	Producer's Accuracy	User's Accuracy
Low coverage	40.87%	71.39%
Medium coverage	86.37%	91.62%
High coverage	84.16%	96.19%
All strata	83.97%	95.38%

The preliminary accuracy analysis showed that, in 2017, the model performed better in regions with higher center pivot coverage. Considering all strata in 2017, the model presented an omission error of 16% and an inclusion error of 5%.

2.6 Results

In terms of pixel area, compared to surveys carried out by *Atlas da Irrigação* (ANA, 2017) and ANA/Embrapa (ANA, 2019a), the mapping of center pivots showed greater agreement in the period from 1985 to 2010. For the years after 2010, Collection 7 underestimated the mapped area by an average of 13% (Figure 9). According to Embrapa data, for example, in 2020, there were about 1.60 Mha of center pivot irrigation areas in Brazil. MapBiomas mapped an area of 1.46 Mha, equivalent to 91% of the total estimated by the agency.

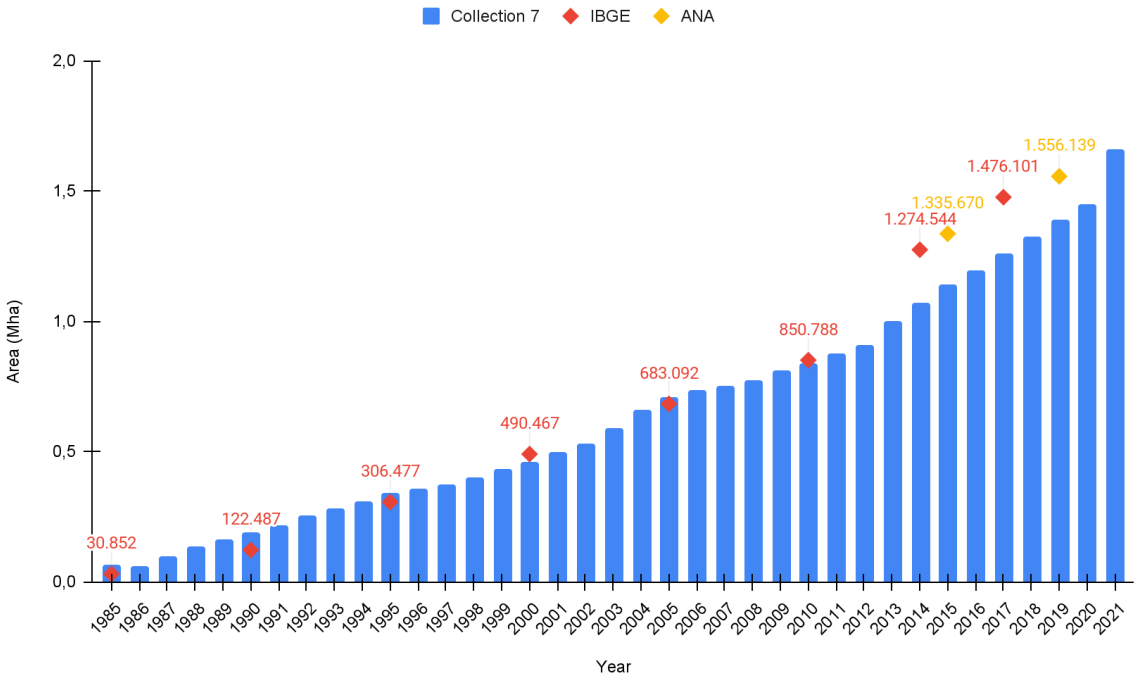

Figure 9: Results of automatic mapping of center pivot irrigation systems in Brazil based on Landsat images for the period from 1985 to 2021 compared to surveys carried out by the *Atlas da Irrigação* (ANA, 2017, 2021a) and ANA/Embrapa (ANA, 2019a).

Center pivot irrigation information from Collection 7 show a similar trend observed in irrigation ANA data, which demonstrates a trend of growth in irrigated areas. Furthermore, data from Collection 7 showed that center pivot irrigation area increased about 24 times between 1985 until 2021, reaching 1.68 Mha in the last time series year, while in 1985 the area was about 0.07Mha.

3 Irrigated rice

The mapping of 'Center pivot irrigation systems' and 'Irrigated rice' classes was performed using Landsat imagery and an adapted U-Net architecture (RONNEBERGER et al., 2015), an image segmentation convolutional neural network architecture. The adapted U-Net architecture was trained with two different sets of samples, one set with center pivot

irrigation systems samples and other with irrigated rice samples. To increase the temporal and spatial consistency of the final maps, the raw result was post-processed using temporal and spatial filters (Figure 10).

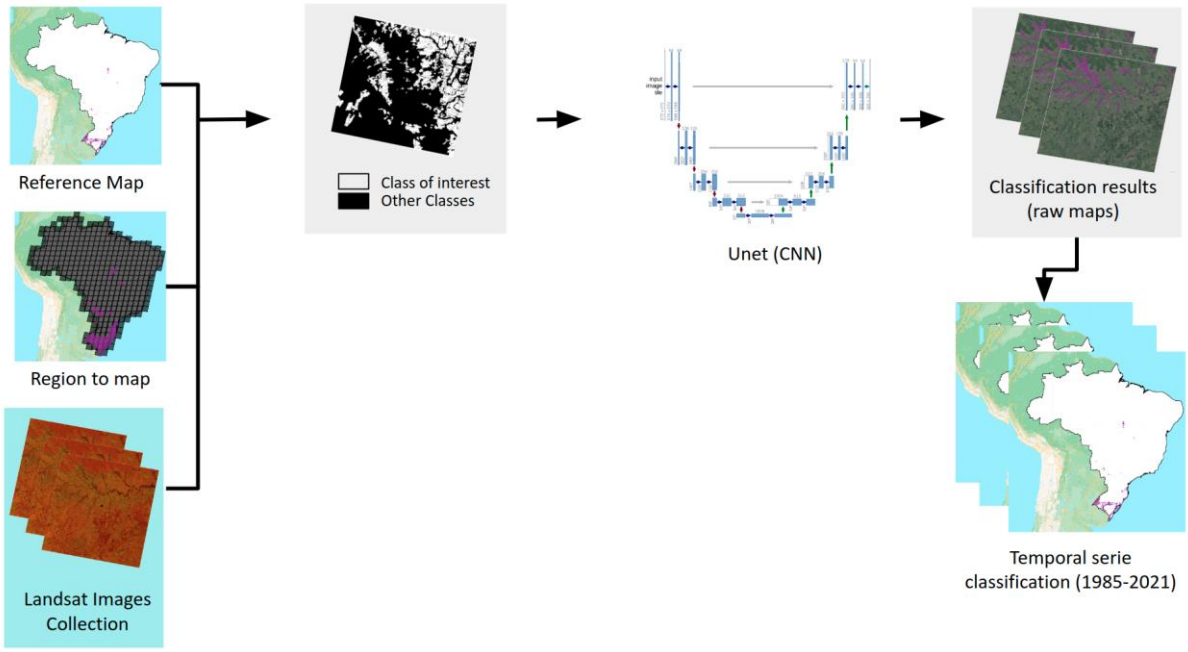

Figure 10. Classification process for mapping center pivot irrigation systems and irrigation rice in MapBiomas Collection 7.

3.1 Image selection

Due to the different agricultural dynamics, cropping systems, soil management and vegetation dynamics of Brazilian biomes, added to the computational limitation (which prevents the use of different images and their attributes), different models were trained from specific mosaics for each region to allow these mosaics to more prominently highlight the rice plots and aid model training. Therefore, three types of mosaics were created to train three different models, one for each Brazilian state. To create the mosaics, images were first obtained from the Collection 1 Tier TOA collections of the TM sensors (from Jan/2000 to Oct/2011), ETM+ (from Jan/2000 to May/2003 and from Oct/2011 to Mar/2013) and OLI (from Mar/2013 to Dec/2019). Then, images of the growing season and off-season of irrigated rice were selected depending on the region. The next step was the elimination of clouds and cloud shadows from the images through the information contained in the Landsat quality band metadata (QA band).

The selection of images was made based on the growing season and off-season periods according to the year of mapping carried out in each state (Table 3).

Table 3. Periods used for the selection of images that were used to compose the mosaics used for the mapping of irrigated rice in Collection 7.

State	Start season	End season	Start off-season	End off-season
Tocantins - TO	04/01/year	07/30/year	08/01/year-1	11/01/year-1
Rio Grande do Sul - RS	10/01/year-1	04/01/year	01/10/year-1	01/01/year
Santa Catarina - SC Paraná - PR	10/01/year-1	04/30/year	01/01/year	07/30/year

3.2 Definition of regions for classification

The delimitation of the mapping area was based on the map of irrigated rice in Brazil published by the National Water Agency (ANA, 2021b) and the National Supply Company (Conab) in 2020. The selection of images was made based on the season period according to the year of mapping carried out in each state. The reference map was divided into blocks of 0.5 x 0.5 degrees (~300 thousand ha each). The blocks used for irrigated rice mapping and training were those that overlapped the reference map and with the states of interest of Collection 7, as illustrated in Figure 11.

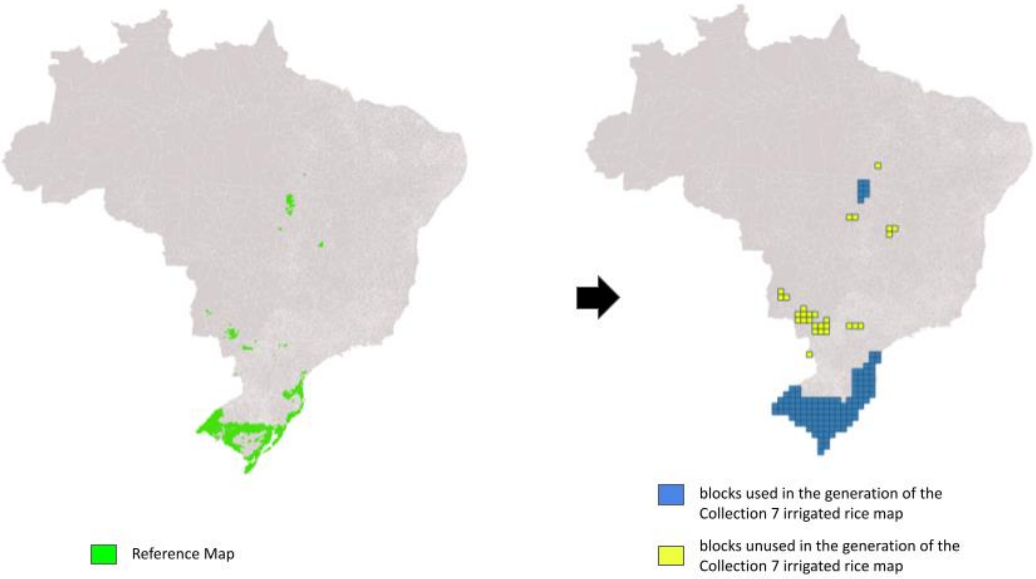

Figure 11. Study area used for the mapping of irrigated rice in the MapBiomas Project.

3.3 Classification

3.3.1 Classification scheme

Each of the three Brazilian states chosen was mapped by a model specifically trained for that region. The classification considered two classes (binary classification), 1 for 'Irrigated rice' and 0 for 'background'.

3.3.2 Feature Space

The feature space for irrigated rice mapping using the adapted U-Net architecture was selected to ensure the greatest highlight between irrigated rice crops and other land uses (e.g. other types of agricultural crops). The variables were selected according to the Brazilian state to be mapped, as shown in table 4.

Table 4: Bands, indexes, and metrics used to compose the Landsat mosaics to classify rice.

State	Tocantins	Santa Catarina	Paraná	Rio Grande do Sul
Bands	SWIR1, SWIR2	SWIR2	SWIR1, SWIR2	SWIR1, SWIR2, TIR1
Indexes	EVI2, NDWI	EVI2, NDWI	EVI2, NDWI	EVI2
Metrics	CEI (EVI2), CEI (NDWI)	CEI (EVI2), CEI (NDWI)	CEI (EVI2)	CEI (EVI2)
Period	Bands - off season CEI - Annual	Bands - off season CEI - Annual	Bands - off season CEI - Annual	Bands - season CEI - Annual

Figure 12 illustrates the different image mosaics that were used to map irrigated rice in the different Brazilian states evaluated.

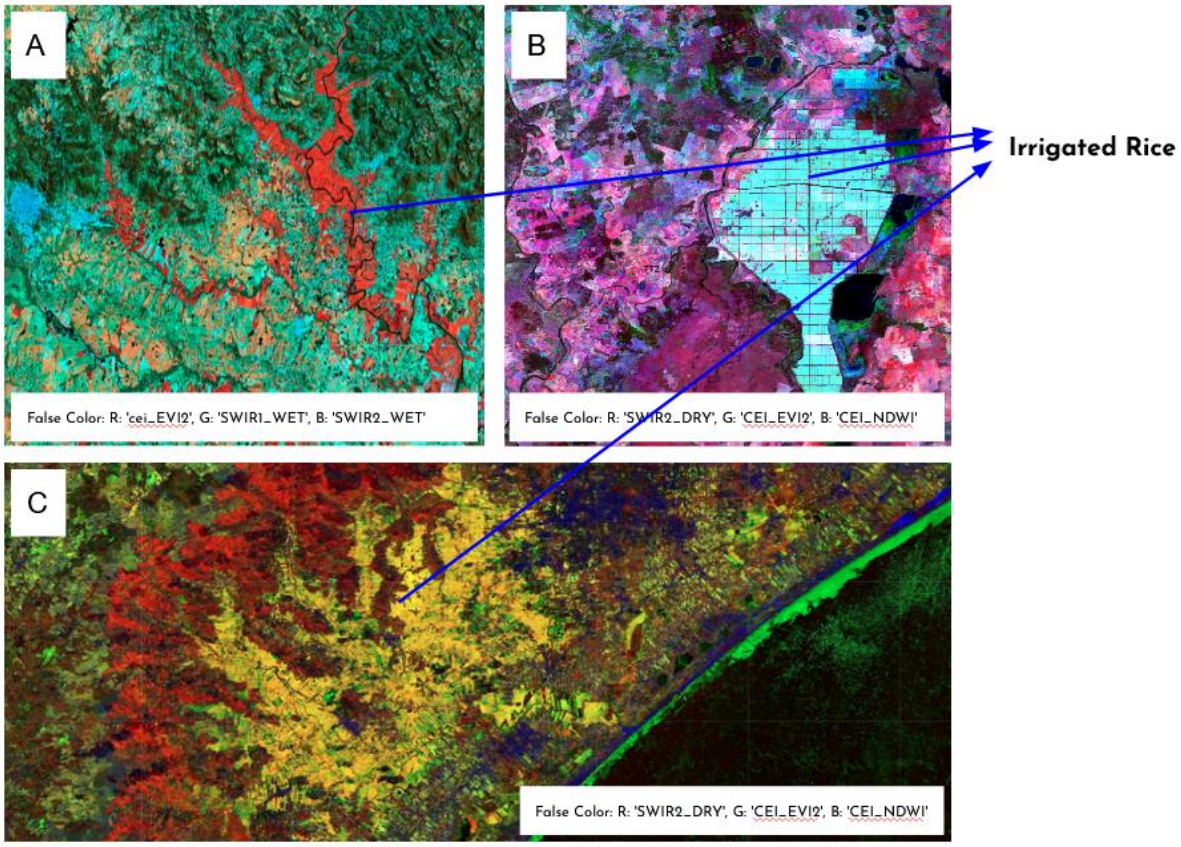

Figure 12. RGB visualization of the mosaics used for the mapping of irrigated rice in the states of Rio Grande do Sul (A), Tocantins (B) and Santa Catarina (C).

3.4 Classification algorithm, training samples and parameters

To obtain the training, validation and test sets, each of the training blocks was first traversed with a moving window, generating chips with 256 x 256 pixels. Then, for each block, the generated chips were divided into 70, 20 and 10% for training, validation and test sets, respectively. The training and validation datasets were used in the model adjustment and pre-validation processing during model training, while the test dataset was used only for final validation of the already trained model.

After the separate data sets, the pixel values of each feature were normalized. The normalization rescaled the numerical values of the features to the range 0 to 1, making each feature contribute similarly to the calculation of model loss. In Figure 13, an example of the mosaic and its respective reference map is shown.

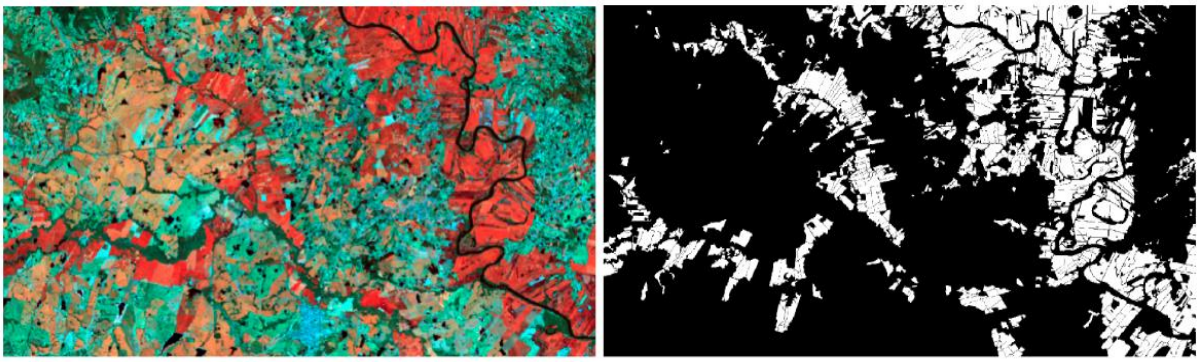

Figure 13. Example of an image mosaic used to train one of the models and its respective ground truth containing classes 1 (irrigated rice) and 0 (background).

After the models were trained, the classification of irrigated rice in the different states was performed for each year of the period 1985-2021.

3.5 Post-Classification

In the post-processing of irrigated rice, an exclusion filter was not used, since the map resulting from U-Net is less subject to isolated noise, when compared to the map resulting from pixel-by-pixel algorithms such as Random Forest, for example. Temporal filters were also not applied to the rice map, as its planting dynamics, especially in the Pampa biome (largest area of rice in Brazil) where rice areas are rotated with cattle and fallow, cannot be neglected..

3.6 Validation strategies

It was carried out an analysis of the model's accuracy on the chips that were allocated in the dataset of the test. The metric adopted for the initial validation was the Dice Coefficient. The Dice Coefficient represents **2 * the Area of Overlap divided by the total number of pixels in both images** with values ranging from 0 to 1, with 1 signifying the greatest similarity between predicted and truth.

Table 5. Metrics used to classify irrigated rice in MapBiomas Collection 7.

Region	Evaluated chips	Dice Coefficient
Rio Grande do Sul - RS	536	0.69
Santa Catarina - SC	140	0.44
Tocantins - TO	288	0.40

The result of the model evaluation and the visual inspection of the mapping results indicate that the model had a better performance in the state of Rio Grande do Sul, a region with most of the irrigated rice area. Regarding the detailing of the mapping, the model had greater difficulty in delimiting the borders of the agricultural plots, which may partially justify the values of the Dice Coefficient.

The area resulting from the automatic mapping of irrigated rice from Collection 7 was compared with the area of total and irrigated rice, adapted from the "Levantamento Sistemático da Produção Agrícola - IBGE 1986-2020" (EMBRAPA, 2020) (Figure 14). The results informed, in general, an underestimation around 45% of Collection 7 compared to IBGE data. These differences in rice area are higher over 1986 until 2014, when the underestimation was about 52%. However, from 2015 to 2020 Collection 7 reached an underestimation around 11%, mapping from 77 to 114% of the IBGE surveys.

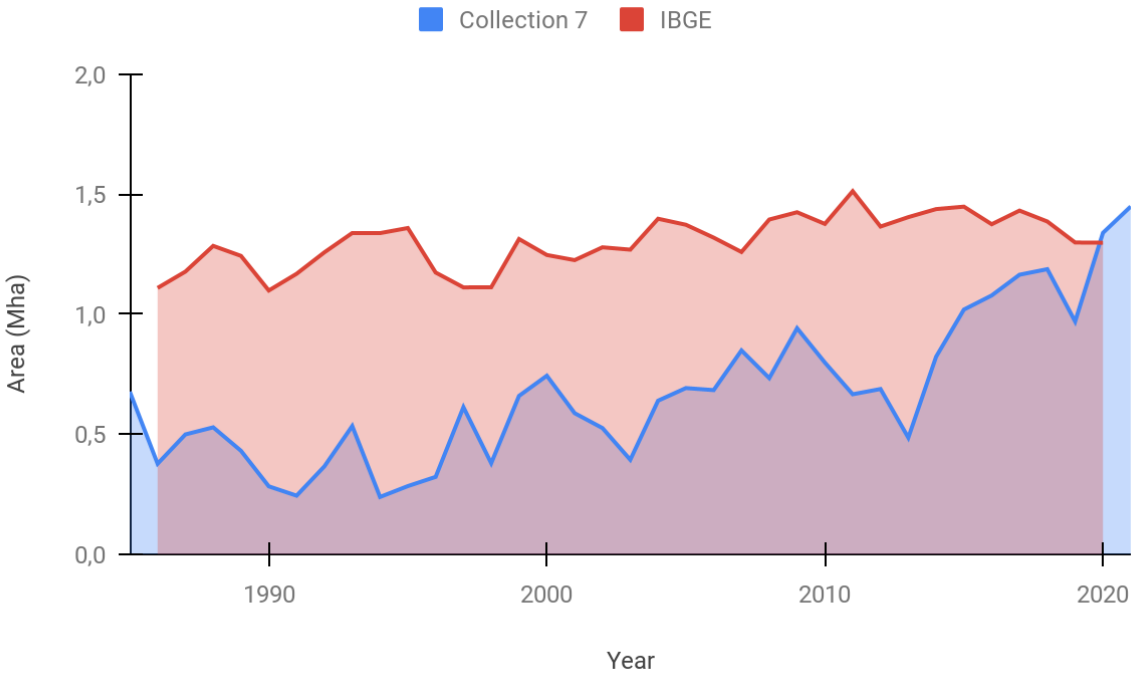

Figure 14. Comparison between rice areas obtained from the MapBiomas Collection 7 and data provided by the Levantamento Sistemático da Produção Agrícola - IBGE (1986-2020).

4 Irrigated agriculture in semi-arid region

The 'Other irrigation systems' class was mapped only for some municipalities in the Brazilian semi-arid region using the Random Forest classifier (BREIMAN, 2001). The process used was similar to that used to map the 'Center pivot irrigation systems' class. The main differences are in the generation of samples, which uses a semi-automatic approach based on agriculture maps and estimates of the irrigated area by Brazilian municipalities (Figure 15).

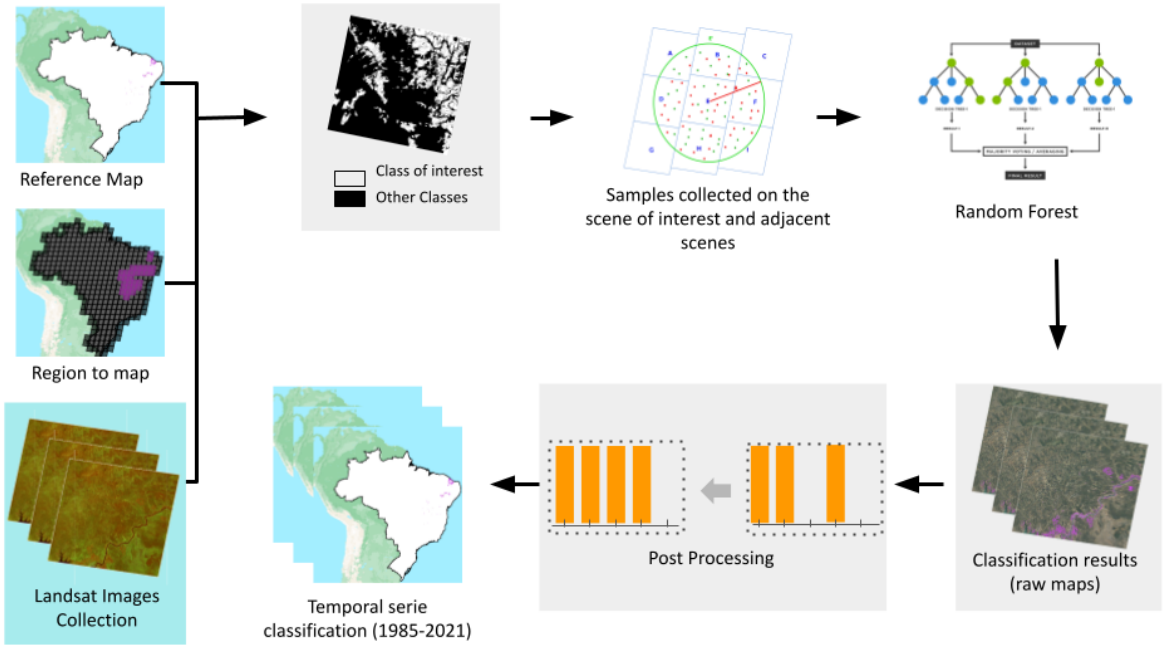

Figure 15. Classification process for mapping 'Other irrigation systems' in MapBiomas Collection 7.

4.1 Image selection

The mapping of irrigation in semi-arid region used normalized Landsat mosaics, a reflectance normalization product based on Landsat imagery and the Moderate-Resolution Imaging Spectroradiometer (MODIS) products (see Appendix of Agriculture and Forest Plantation). In addition to the normalized Landsat mosaics, data from Shuttle Radar Topography Mission - SRTM (FARR et al., 2007) and climatic data from TerraClimate (ABATZOGLOU et al., 2018) were used.

4.2 Definition of regions for classification

In the mapping of other irrigation systems, the study area was restricted to the Brazilian semi-arid region. In this region, due to water requirements, irrigation is almost a mandatory requirement to reduce production risks and/or increase productivity.

According to the 'Atlas da Irrigação' (ANA, 2017), in 2015, of the 1262 municipalities that make up the Brazilian semi-arid region, only 19 had at least 5,000 hectares of irrigated

agriculture. Together, these 19 municipalities are responsible for approximately 315 thousand hectares (44%), out of the total of 708 thousand hectares that make up the irrigated area of the Brazilian semi-arid region. Due to the lack of reference maps available on this topic, and because it is a first effort, the mapping was carried out in these 19 municipalities with the most significant amount of irrigated agriculture in the region. In addition to these, another 15 municipalities in the states of Bahia and Pernambuco located around the São Francisco River were included in the mapping area. These 15 municipalities are located in a region considered an important fruit center production in Northeast Brazil. Figure 16 shows the spatial distribution of the 34 municipalities to map 'Other Irrigation System' class.

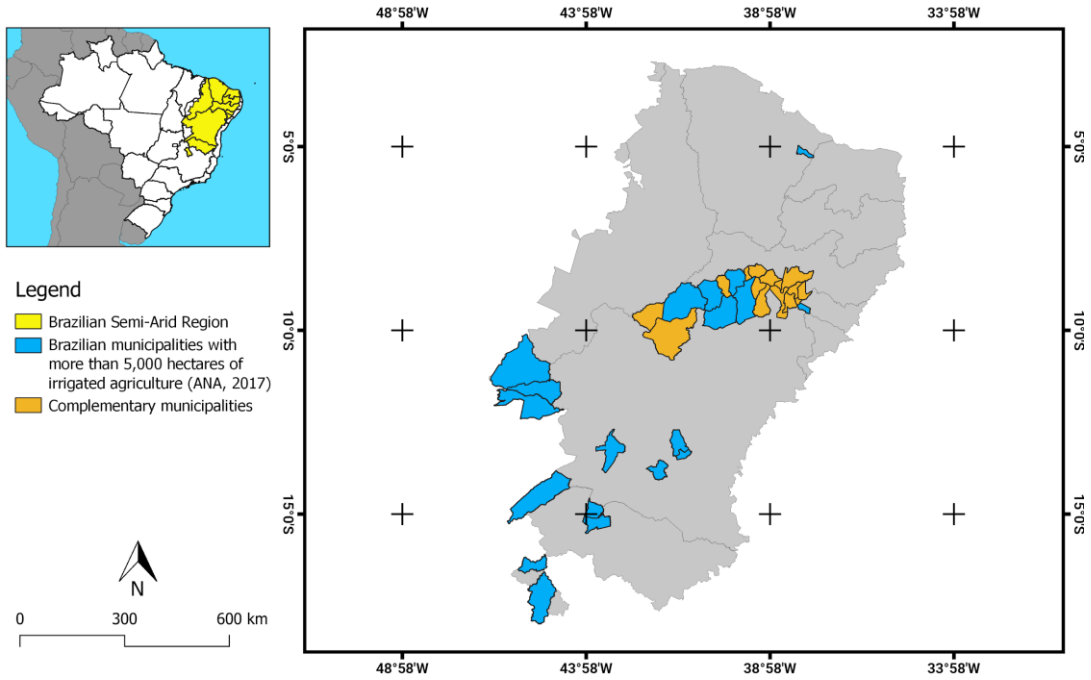

Figure 16. The municipalities used to map 'Other Irrigation Systems' class in the Northeast of Brazil.

4.3 Classification

4.3.1 Classification scheme

The irrigated areas in the semi-arid region are composed of the mapping of the 'Center pivot irrigation systems' class, in which the methodology was presented in Section 2, and the mapping of the 'Other irrigation systems' presented in this section.

The mapping of 'Other irrigation systems' class considered three possible classes, 'Irrigated agriculture', 'Non-irrigated agriculture' and 'Non-agriculture'. The regions that were mapped by both methodologies and allocated to the classes 'Center pivot irrigation systems' and 'Irrigated agriculture', were reclassified to the class of 'Center pivot irrigation systems'. The regions that were mapped as 'Irrigated agriculture', but were not mapped as 'Center pivot irrigation systems', were converted to the class 'Other irrigation systems'.

4.3.2 Feature space

For mapping of other irrigation systems, in addition to the data available from the Landsat program satellites, auxiliary metrics from other sources were added. The slope, with 30 meters of spatial resolution, was derived from the elevation obtained in the digital terrain model Shuttle Radar Topography Mission - SRTM (FARR et al., 2007). The actual evapotranspiration, precipitation, and water requirements, with approximately 4 kilometers of spatial resolution, were derived from climatic data obtained from the TerraClimate (ABATZOGLOU et al., 2018), a set of monthly climate data and water climate balance for the global land surface. Auxiliary metrics can complement the information obtained by optical sensors and assist in the identification of irrigated agriculture (DEINES et al., 2019). Table 6 presents the set of annual metrics used to map irrigated agriculture in the Brazilian semi-arid region.

Table 6. Set of metrics used to map irrigated agriculture in the Brazilian semi-arid region.

Source	Bands and Spectral indices	Metrics
Landsat	RED NIR SWIR1 TIR1 EVI2 (JIANG et al, 2008)	EVI2 Quality Mosaic, Minimum, Median , and standard deviation values

	NDWI (GAO, 1996) CAI (NAGLER et al, 2003)	
SRTM (FARR et al., 2007)	Slope	--
TerraClimate (Abatzoglou et al., 2018)	Actual Evapotranspiration Precipitation Water Requirements	Accumulated

4.4 Classification algorithm, training samples and parameters

Due to the absence of georeferenced reference data on irrigated agriculture and the hydrological characteristics in the Brazilian semi-arid, the premise adopted was that crops with greater vegetative vigor are those that received irrigation at some time of the year, which this directed collection of samples from training.

The collection of samples for the training of the classification model was carried out for the years 2016 and 2017 in the selected municipalities, and followed the steps:

1. samples from three classes were collected: 'Irrigated Agriculture', 'Non-irrigated Agriculture' and 'Non-Agriculture';

2. Agriculture maps produced by Agrosatélite for the harvest 2016/2017 were used for the sample collection. The samples of the classes 'Irrigated Agriculture' and 'Non-irrigated Agriculture' were obtained inside of the agriculture map, and the samples for the class 'Non-agriculture' were obtained outside of the agriculture mask.

3. for the 'Irrigated Agriculture' class, a mask of the regions with the highest annual values of the EVI2 vegetation index was created so that the area (in acres) of the chosen regions was close to the irrigated agriculture area of the municipality according to the *Atlas da Irrigação* (ANA, 2017) and the *Censo Agropecuário* (IBGE, 2019);

4. for the 'Non-irrigated Agriculture' class, regions located within the agriculture mask were selected that were not chosen for the 'Irrigated Agriculture' class;

5. stratified sampling of one thousand points was carried out for each 100 thousand hectares of the area of each municipality and as a criterion for sampling the percentage of the area of each class.

For the classification process of other irrigation systems areas, the Random Forest classifier was used. The parameters used in Random Forest are shown in Table 7.

Table 7. Parameters used in Random Forest for the classification of other irrigation systems in the semi-arid region in Brazil.

Parameter name	Value
Decision trees	100
Samples	1,000 samples for every 100,000 hectares
Variables	32 variables
Variables per split	$\sqrt{Number\ of\ Variables}$
Classes	3 classes

One classifier was trained per municipality, with samples collected in the years 2016 and 2017 and used for the classification from the years 1985 to 2021. The classification result contains the three classes: 'Irrigated agriculture', 'Non-irrigated agriculture' and 'Non-agriculture'. The 'Irrigated agriculture' class does not differentiate the types of irrigation systems, so in post-processing, the pixels mapped as center irrigation pivots in the specific approach for mapping center irrigation pivots were removed from the 'Irrigated Agriculture' class, remaining only the other irrigation systems.

4.5 Post-Classification

The post-classification process of irrigation agriculture maps included the application of temporal and spatial filters.

4.5.1 Temporal filter

In the other irrigation systems mapping, a moving five-year window was also used, but using a different rule from the center pivot irrigation systems. In this filter, if the evaluated pixel was in the same class as at least three other pixels (previous, ahead or both), it remains in that class. However, if the evaluated pixel was not of the same class as at least three pixels (previous, ahead or both), the class was changed.

4.5.2 Spatial filter

In the other irrigation systems a convolutional spatial filter was used, with a 5 x 5 kernel, to remove or add the filtered pixel (central pixel) to the mapping result.

4.6 Validation strategies

Due to the absence of georeferenced reference data for the "Other Irrigation System" class, Collection 7 does not have an accuracy analysis for this class. In terms of the pixel area, Figure 17 presents the mapped area of irrigated agriculture in the 34 selected Brazilian municipalities compared to surveys carried out by the *Atlas da Irrigação* (ANA, 2017, 2021a) and the *Censo Agropecuário* (IBGE, 2009, 2019). It is important to emphasize that the map of other irrigation systems in the semiarid region is still a beta version, so its data should be used with caution.

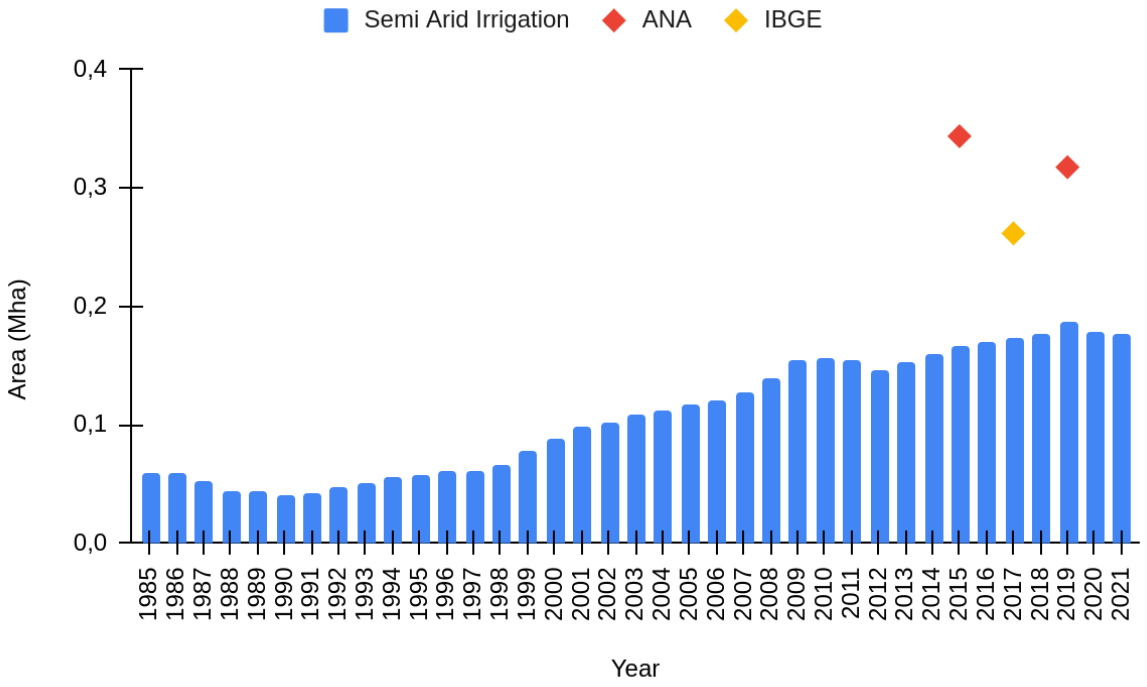

Figure 17. Results of the automatic irrigation mapping of the 34 Brazilian municipalities chosen in the study area for the period from 1985 to 2021 compared to surveys carried out by the *Atlas da Irrigação* (ANA, 2017, 2021a) and the *Censo Agropecuário* (IBGE, 2009, 2019).

Center pivot irrigation information (*Beta*)

Understanding center pivots irrigation dynamics allows us to improve our understanding about most parts of irrigated agriculture in Brazil. The first effort to understand irrigation systems in the MapBiomas project began in Collection 5, with the use of innovative methods of Artificial Intelligence, through convolutional artificial neural networks to perform semantic segmentation of pivots throughout the Brazilian territory. In Collection 6 there was an expansion of the years mapped, with generation of time span maps of the entire MapBiomas series. In Collection 7 in addition to another time series expansion of center pivot irrigation map, covering from 1985 until 2021, it was also made effort to improve our understanding about crop dynamics in center pivot irrigation. Thus, in Collection 7 of MapBiomas, a methodology was developed to provide more detailed information about this system, such as the number of cycles performed per pivot in the crop year, the dates of start and end of each cycles, in addition to information about accumulated precipitation in each pivot and each crop cycle.

4.7 Overview of the classification method

To provide this information to each pivot, several steps are necessary, from applying a Deep Learning model for center pivots irrigation individualization to obtaining smoothed time curves to identify the number of annual cycles existing in each of these pivots. The FIgure 18 presents all steps of these methodology.

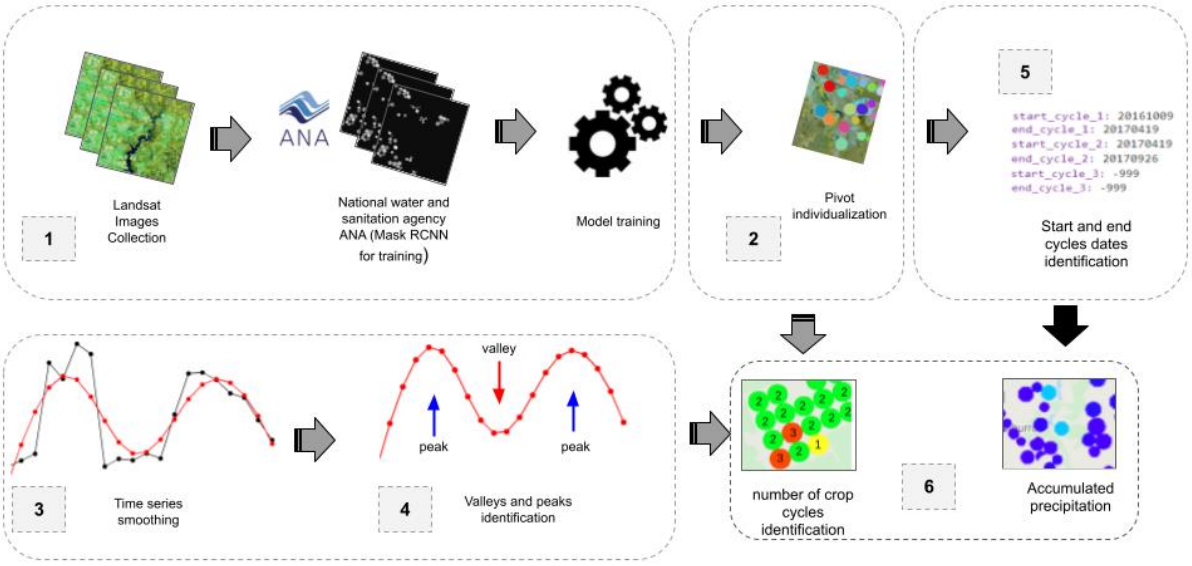

Figure 18. Flowchart of the methodology necessary to obtain the number of cycles per pivot. 1) Obtaining the training dataset for the neural network (Landsat image and Mask of pivots); 2) Training the Deep Learning model for individualization of the pivots; 3) Landsat time series curve smoothing; 4) Identification of peaks and valleys in the curve; 5) Identification of the

start and end dates of each cycle; and 6) Obtaining number of crop cycles and accumulated precipitation per cycle per pivot.

4.8 Center pivot individualization

4.8.1 Image selection

To individualize each center pivot irrigation in Minas Gerais we used annual mosaics generated from available images in each year. Therefore, images from the Landsat series were obtained on the Google Earth Engine platform (Collection 1 Tier 1 TOA) in the period of 2015 to 2021. Only images with under 80% of cloud cover and shadows were considered.

4.8.2 Definition of regions for classification

Minas Gerais is the initial region to generate the center pivot irrigation information, since this state has the largest number of pivots in Brazil. To individualize each center pivot irrigation in Minas Gerais, samples were first selected that represent relevant information about the pivots, so it was decided to select the blocks that contained at least 5 pivots. Thus, the samples were stratified between test areas (blocks with at least 5 and at most 9 pivots) and training areas (blocks with more than 10 pivots). Figure 19 presents Minas Gerais state location, as well as the blocks used for the RCNN (Region Based Convolutional Neural Networks) Mask prediction. The Mask R-CNN is a Convolutional Neural Network (CNN) and state-of-the-art in terms of image segmentation. This variant of a Deep Neural Network detects objects in an image and generates a high-quality segmentation mask for each instance.

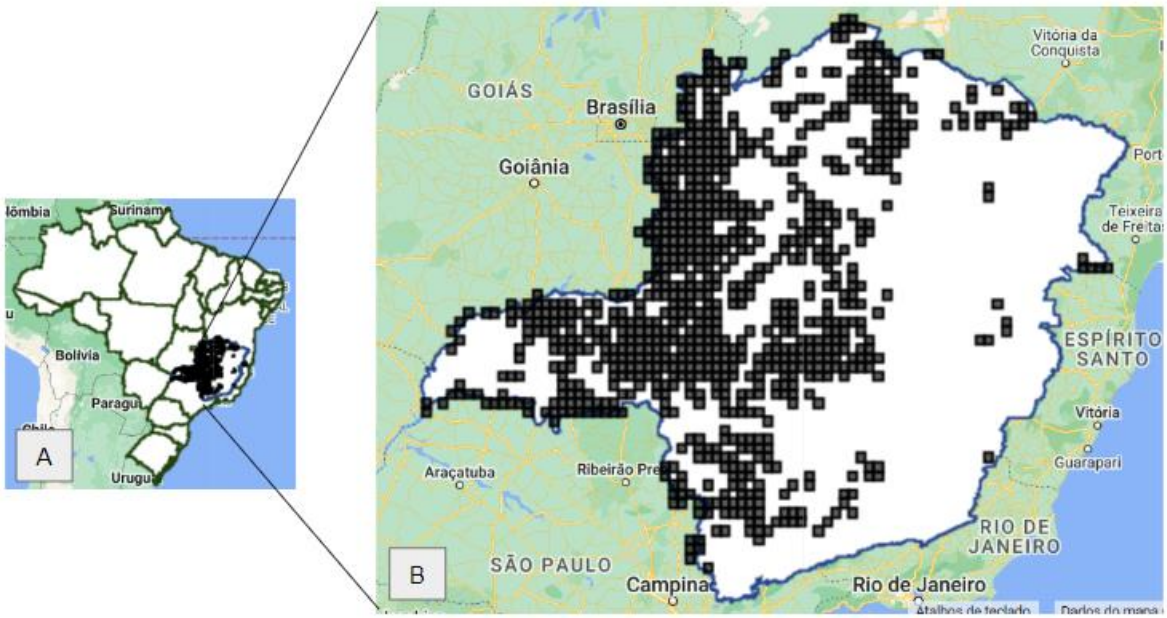

Figure 19. A) Minas Gerais state in Brazil, B) Minas Gerais and tiles (grid in black) for RCNN Mask prediction. Note: Areas without tiles indicate the non-existence of irrigation center pivots, according to the map made available by ANA for the year 2019.

4.8.3 Classification

4.8.3.1 Classification scheme

A RCNN was trained to identify and individualize each center pivot irrigation in Minas Gerais state. Semantic segmentation considers two classes, (binary classification), 1 for 'pivot' and 0 for 'non pivot', in instance segmentation each pivot is mapped separately, adding one unique ID for each.

4.8.3.2 Feature space

The Normalized Difference Vegetation Index (NDVI) (ROUSE et al., 1974) was calculated for each image in order to generate standard deviation and percentiles metrics, as presented by Table 8. These metrics were chosen seeking to capture not only the temporal variation of NDVI in the pivots, but also the variations of other agricultural targets outside of pivots (such as pasture, barren soil, native vegetation, etc).

Table 8. Index and metrics used to individualize center pivot irrigation in MapBiomas Collection 7.

Indexes	NDVI
Metrics	stdDev, 75th percentile, 100th percentile

4.8.3.3 Classification algorithm, training samples and parameters

Instance segmentation is performed from a pre-trained neural network of Mask RCNN type architecture. This architecture was developed in Python, using the Pytorch framework, along with the Detectron 2 package. Figure 20 represents the flowchart of the entire Mask RCNN training process.

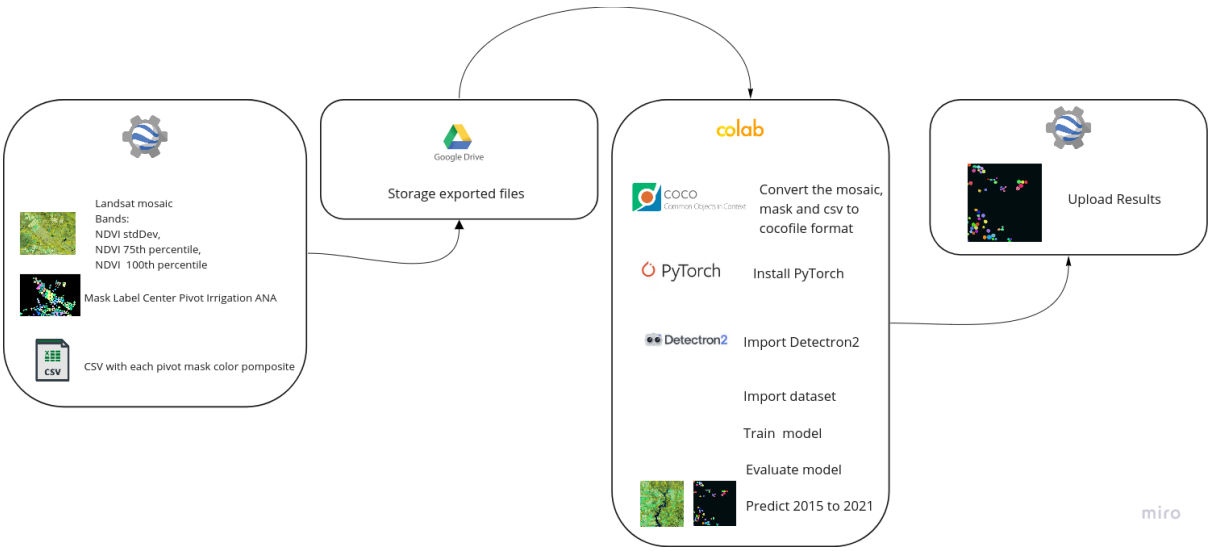

Figure 20. Pipeline to use Detectron2 to pivot instance segmentation.

4.8.4 Post-Classification

Post processing of the center pivot irrigation has two more steps besides the spatial and temporal filters, which are focused for solving pivots 'union' and 'edge' problems.

4.8.4.1 Union Problem

Union problem consists of a false pivot generated between real pivots that are overlapping. FIgure 21 exemplifies this problem as well as its resolution.

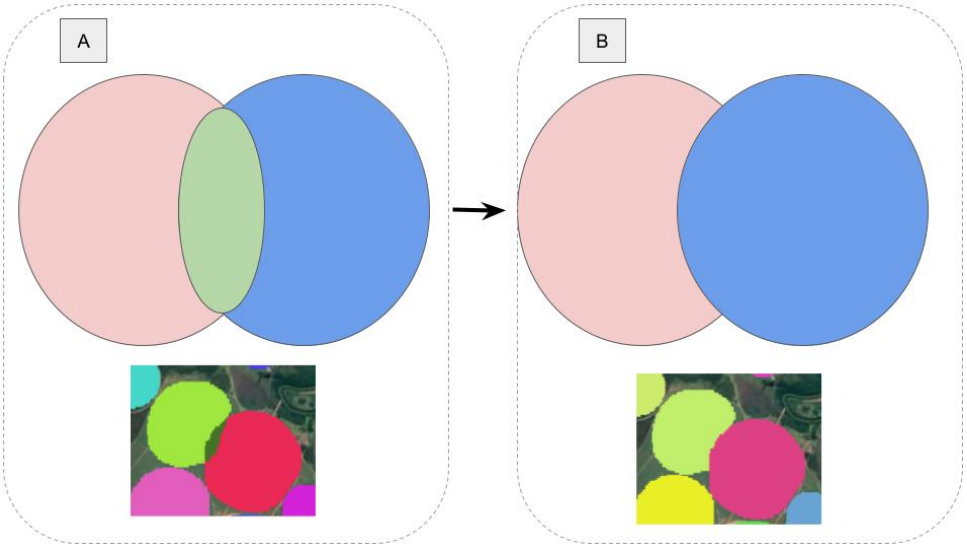

Figure 21. Illustration of the problem of the union between two or more center irrigation poles. A) union problem; B) result of the filter applied to solve the union problem.

To solve this union problem it is necessary to find the ID of the false pivot (generated by union of two or more pivots through a sum of true IDs), and then identify the IDs pivots that generated this false pivot ID. Based on this information it is possible to replace a false ID to a true ID, from one of pivots that generated this false ID.

4.8.4.2 Edge Problem

The edge problem is a result of the shape and size of the RCNN Mask input. Some pivots will inevitably be "cut off" due to the size of the input tiles, i.e. one part of the pivot will be in one block (tile) and the other part will be in another adjacent block. The edge problem was solved with the application of two complementary filters (erosion and dilation) and a reduction by spatial connectivity. Figure 22 shows an example of an application to solve edge problems (A).

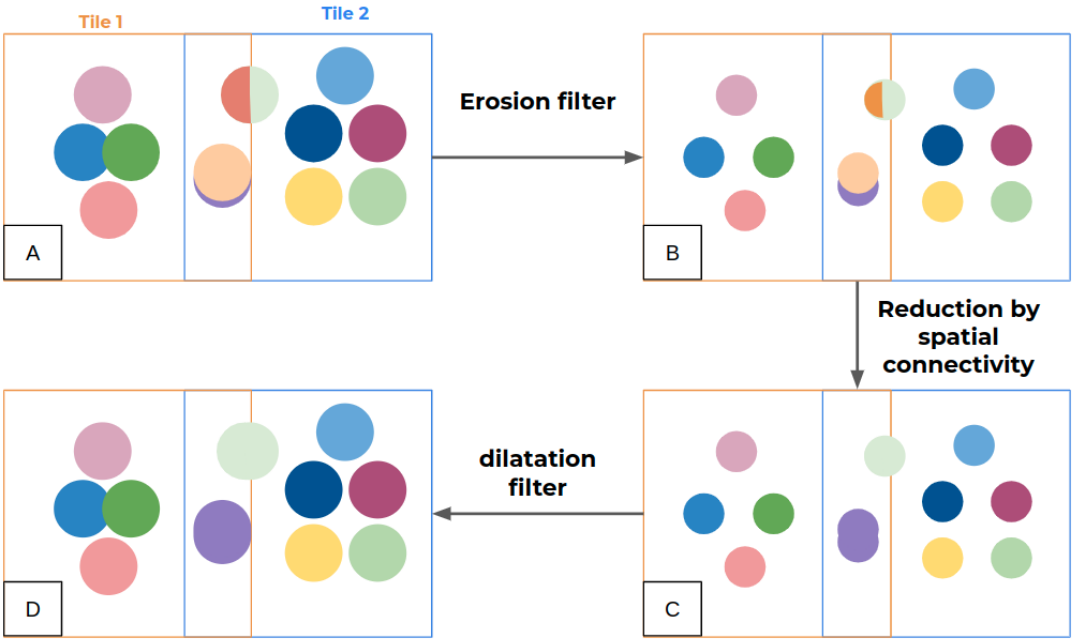

Figure 22. A) Example of application of morphological filter to solve edge problems. A) tiles with pivot edge problems; B) erosion filter; C) spatial connectivity Reduction and D) dilatation filter.

The erosion filter is applied to the tiles in order to reduce the size of the instances (pivots) with the goal of isolating them from each other (B). Then, pivots that were "cut off" by the tile of the RCNN Mask and that exist in the overlap of both boundary images are connected (C). Finally, after this step it is necessary to apply the morphological dilation filter to return pivots to their original size (D) .

4.8.4.3 Temporal filter

For temporal consistency of the IDs over time, a temporal filter was applied with the goal that each pivot remains with the same ID over the years. In this step, a reference image was generated through the accumulation function of all years (2015 to 2021), thus the reference image has all the pivots of the time series and their respective IDs. An accumulation of pivots must be calculated for each year, for example, the accumulation of the year 2020 has the pivots of the years 2015, 2016, 2017, 2018, 2019, and 2020.

4.8.4.4 Spatial filter

A spatial filter was used to remove areas smaller than 10 hectares, so that the noise caused by the accumulation function is excluded, as shown in Figure 23.

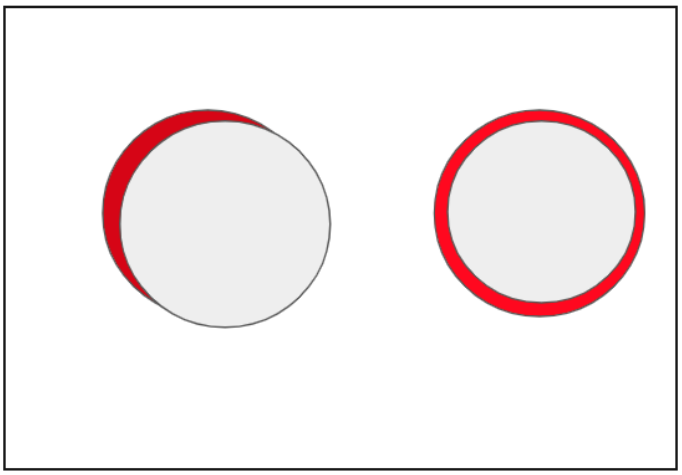

Figure 23. Example of spatial filtering. Pivot polygons in red noise generated by the accumulation function that are removed through the spatial filter.

4.8.5 Validation strategies

To validate the instance segmentation (Mask RCNN) and semantic segmentation (Unet) methodologies the Jaccard index was calculated. The Jaccard index (JACCARD, 1901), also known as the Jaccard similarity coefficient or *intersection over union* (IOU), is a statistic used for gauging the similarity and diversity of sample sets and is defined as the size of the intersection divided by the size of the union of the sample sets (Figure 24).

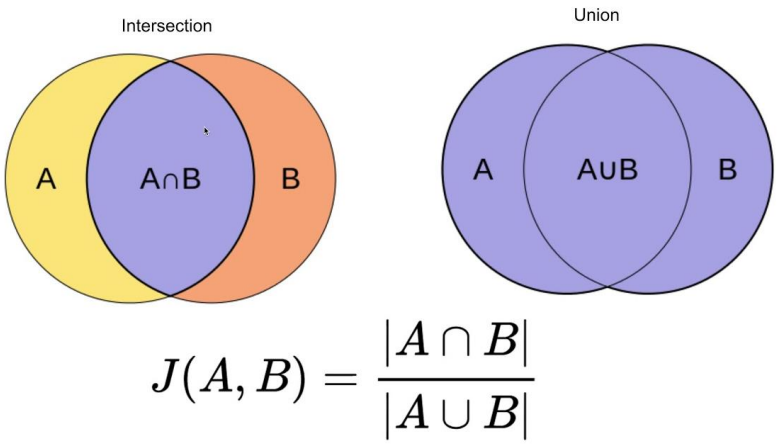

Figure 24: Index Jaccard (IOU) calculation.

The spatial similarity of the Unet results with the Mask RCNN results obtained for the year 2019 was 61.7%. The location data of the center pivots of public irrigation by ANA showed 63.1% similarity with the results obtained from the RCNN Mask. The similarity between ANA and Unet data was 78.4%. It is important to note that instance segmentation is a new methodology that is still under development.

4.8.6 Results

Mask RCNN returns as output a raster of the input mosaic size (15 x 15 km) composed of 0, which corresponds to no detection of center irrigation pivots and values corresponding to the ID of the classified pivots. Figure 25 shows the input and output of the RCNN Mask prediction.

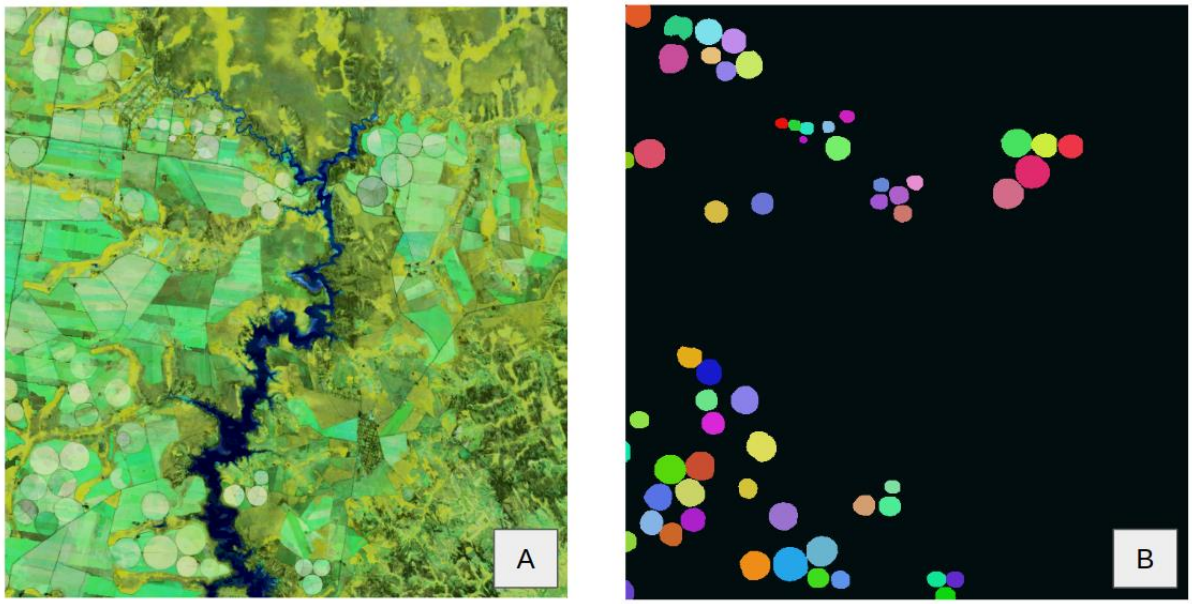

Figure 25. dataset

4.9 Center Pivot Information

Crop and environmental characteristics of center pivot irrigation were obtained to each individual pivot. Thus, using the geometry of each pivot, the following information was extracted: *i*) crop cycles number of each pivot; *ii*) start and end dates of each cycle; *iii*) crop cycle length in days of each cycle; and *iv*) daily average precipitation of each cycle. Besides this, it was also possible to obtain the information if the pivot was in a perennial cultivation area, and if it did not present internal coherence – due to multiple crops at the same time or complex management – , it was not possible to obtain the previous information (*i*, *ii*, *iii* and *iv*) and the pivot is defined as a non-classified.

4.9.1 Image selection

The period used to select the images to obtain a temporal EVI2 curve was based on the crop year. The crop year is different from the conventional year (from January to December), since the crop year aims to define the period when the cultivation occurs in a determined region. Thus, depending on the type of agriculture, the crop year can start in any month of the year, generally following the rainy season, since in this period there is humidity available to the crop development. Thus, to attribute information for each center pivot

irrigation, Landsat images (Collection 1 Tier 1 TOA) were selected from a crop year, in order to compute the EVI2 time series.

The crop year was defined automatically for each Landsat scene and year. We defined the crop year as 3 months before and 9 months after the mean vegetative peak month of each scene, based on an EVI2 curve of MODIS observations. This definition was also used to map temporary crops on MapBiomas Collection 7 and is discussed in more detail in the Agriculture and Forest Plantation Appendix.

It is important to note that, for example, a crop year of 2020 starts around october of 2019 due to the aforementioned seasonal dynamic, so when results for a given year are shown, this should be considered.

4.9.2 Method to attribute information to each pivot

4.9.2.1 Crop cycles number

The first information obtained, that is a base to obtaining the others, was the number of crop cycles of each pivot. An Enhanced Vegetation Index 2 (EVI2) (JIANG et al., 2008) curve of Landsat images from the crop year was smoothed to minimize noise and to reconstruct the time series. The Whittaker method (WHITTAKER, 1922) was used to smooth EVI2 temporal series, since this method presents a great alternative to smooth and to reconstruct temporal series, most importantly keeping only meaningful variations and preserving the temporality of them.

Based on the smoothed EVI2 curve, it was possible to identify when inflections occur in the curve, that is, the change of direction of the curve. Thus, it was possible to identify the points of valleys (defined as the inflections of change from negative to positive sign), and peaks (defined as the inflections of change from positive to negative sign) (Figure 26). Finally, to define the number of cycles, this can be counted as the number of peaks (or valleys minus one), determining the number of crop cycles in a period.

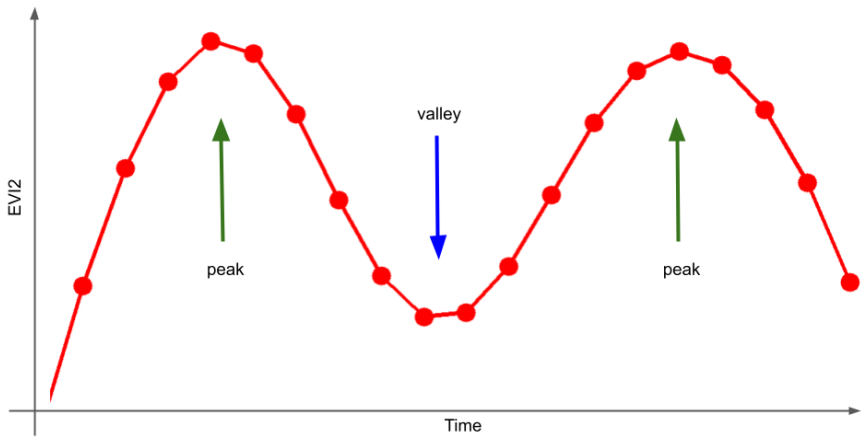

Figure 26: Peaks and valleys identification based on the smoothed EVI2 time series curve.

4.9.2.2 Start and end cycles dates

After identifying the peaks and valleys over the EVI2 time series, it was possible to determine the start and end dates of each cycle. In this step we sought to identify the dates of the valley inflections of the EVI2 curve of each pivot. According to the amount of Landsat images available in the crop year, where each one represents a binary information of valley (1) or no-valley (0), it obtained a percentage of presence of pixels identified as valley (1). Then, after valleys date identification it was checked if the quantity of them was equivalent to the expected quantity for the number of cycles of the pivot (number of cycles +1). If this information is true, the pivot is considered well identified, if not, the pivot is considered as non-classified, since due to the internal dynamics (this usually occurs for pivots with different crops at the same time) it was not possible to identify a spatial coherence in the start and end date definition.

The valley dates were used as a base to determine start and end cycle dates. Based on the daily interval between the two valleys that compose a cycle, the start date was defined as the 20th percentile value, and the end date as the 80th. This was done to reduce cycle coverage to the period where the crops were active, eliminating soil management periods (JÖNSSON and EKLUNDH, 2004). To avoid omitting the planting period, a -15 days buffer was also added to the start cycle dates.

This cycle delimitation method has some known issues, such as the delimitation of cycles based only on the time value. Improvements in this area will be sought for future collections.

4.9.2.3 Crop cycle length

Crop cycle length in days was obtained as a difference between the end and start date of each pivot for each cycle.

4.9.2.4 Average Daily Precipitation

For Precipitation information we used data from Climate Hazards Group Infrared Precipitation with Stations (CHIRPS) product (FUNK et al., 2015), that provide daily and sub-daily precipitation information for quasi–global spatial coverage (50°S-50°N), from 1981-present, in a 0.05° x 0.05° of spatial resolution. Based on CHIRPS data it was obtained an accumulation precipitation of each pivot and then this amount of precipitation was divided by the number of the days of each cycle, resulting in an average daily precipitation per cycle.

4.9.2.5 Additional Information

In addition to the number of crop cycles, start and end dates, and precipitation information, the product also provides additional information about non-classified, perennial and sugarcane pivots.

Perennial and sugarcane pivots were identified using the respective maps from MapBiomas Collection 7, since cycles and environmental information were only accounted for temporary crop pivots.

Pivots in which it was not possible to identify the start and end dates of each cycle were set as non-classified. This problem can be due to a number of factors. For instance, pivot internal crop dynamics, when there are multiple crops on a single pivot, or the same type of crop, however at different times. There is also the possibility of errors inherited by the individualization of pivots methodology, since a not well-defined geometry may encompass other land uses or surrounding crops. In these situations, it was not possible to identify coherent start and end dates, since there is no agreement inside the pivot geometry. Figure 27 presents some examples of when it is possible to identify start and end dates and when this identification is not possible, resulting in non-classified pivots.

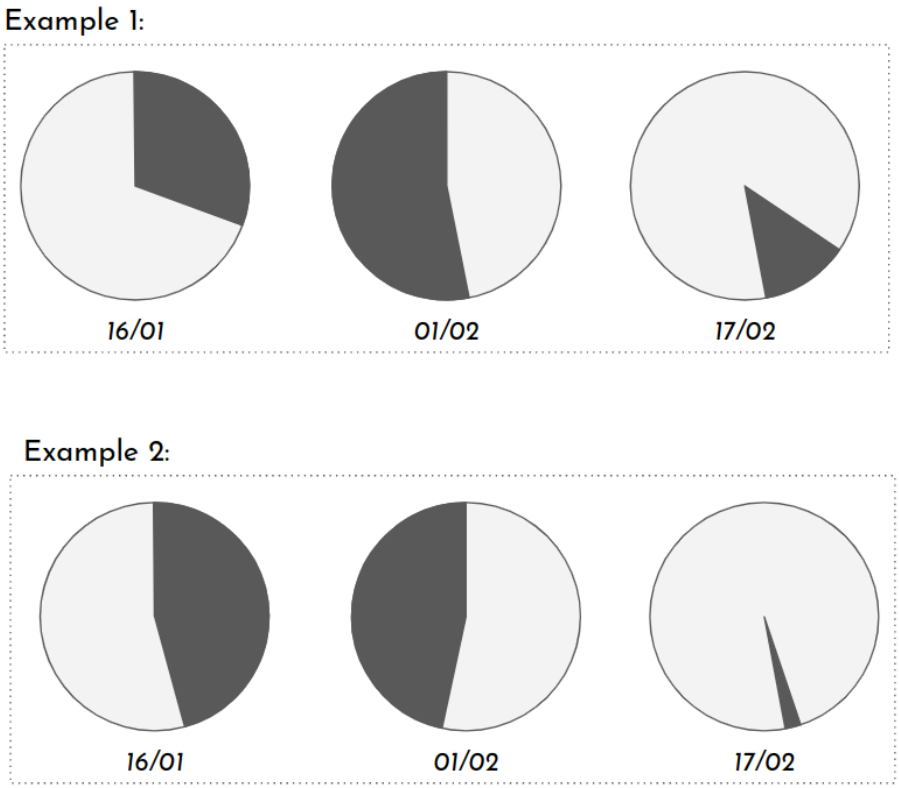

Figure 27: Examples of start and end dates identification, and limitations that cause non-classified pivots.

Example 1 shows a pivot in three different Landsat dates. The shaded area represents the area identified as a valley date. In the first image (16/01) there are approximately one quarter of the pivot identified as a valley. This amount is even less in 17/02. However, in the second date (01/02), most of the pivot was identified as a valley, providing a valley date information.

Example 2, on the other hand, presents a more complex situation. In these three dates (16/01, 01/02, and 17/02), there is not a single image where most of the pivot is identified as valley. In this situation there is no possibility to obtain start and end dates by the same method as before (statistical mode), so pivots in this or similar situations were set as non-classified. This is a known flaw in the methodology and improvements will be sought in future collections.

4.9.3 Validation strategies

From the total of classified pivots, 250 of them were randomly selected and evaluated year by year, visually, in order to validate the consistency in terms of class, start and end dates of each cycle, and also the consistency of number of cycles. This total (250) represents between 3 to 6% of total pivot amount, depending on the year, since the number of pivots increases over the years.

The following errors were considered: (1) cycle number errors, when a pivot shows a difference between the number of cycles identified in the methodology and the visual analysis; (2) dates errors, when the pivot has at least one cycle where the start and end dates are not consistent with the expected in the vegetation index curve; (3) class errors, where the pivot was misclassified in any way. The first two errors can occur at the same time, and when so it is likely that the pivot was mostly not well defined. However, the errors individually do not indicate that the pivot is entirely wrong. Class errors can be associated with an omission from the sugarcane and perennial masks. Cycle number and date errors individually show that a cycle in the pivot was misidentified in some way, but not necessarily all of its cycles. Figure 28 presents the rates (%) of pivot without any kind of error, with only one error and with two errors.

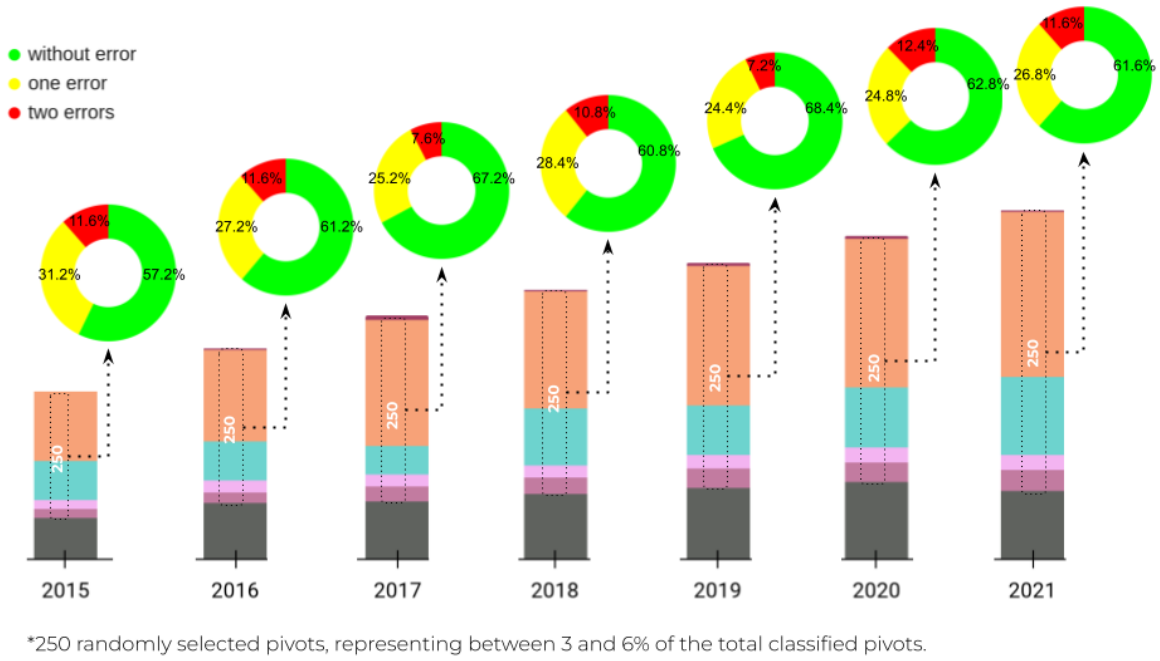

Figure 28: Percentage of pivots without errors, with only one error and with two errors identified in 250 pivots selected randomly.

The results presented in the Figure 28 above, show that about 57.2 to 68.4% of pivots randomly selected have none of the analyzed errors, while around 24.4 to 31.2% of samples presented only one error, and 7.2 to 12.4% of data evaluated presented two types of errors. The analysis also provides information about the type of these errors identified. Figure 29 presents the error rates identified by the pivots sample randomly selected.

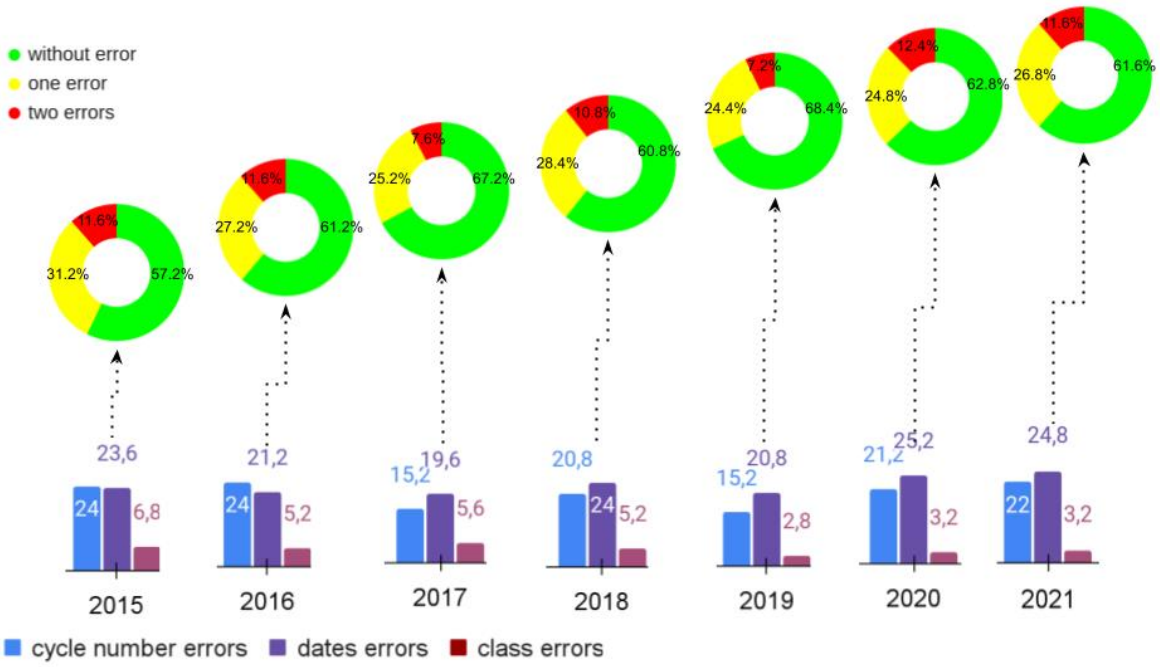

Figure 29: Percentage of type of errors identified in 250 pivots selected randomly.

Figure 29 informs us that we have two main types of errors on pivots. For instance, errors due to incorrect cycle accounting are about 15 to 25% of the errors identified. About 19.6 to 25.2% of errors are related to errors in identifying the start and end dates of cycles, and less than 7% of errors are related to errors in pivot class, i.e. classification of the type of use and coverage of that pivot.

4.9.4 Results

The results obtained for Minas Gerais state are presented in Figures 30 and 31. In Figure 30, the distribution of pivot wich 1 to 3 cycles is displayed over the state area. In Figure 31, the evolution of the number of pivots in each class is shown over the analyzed time period.

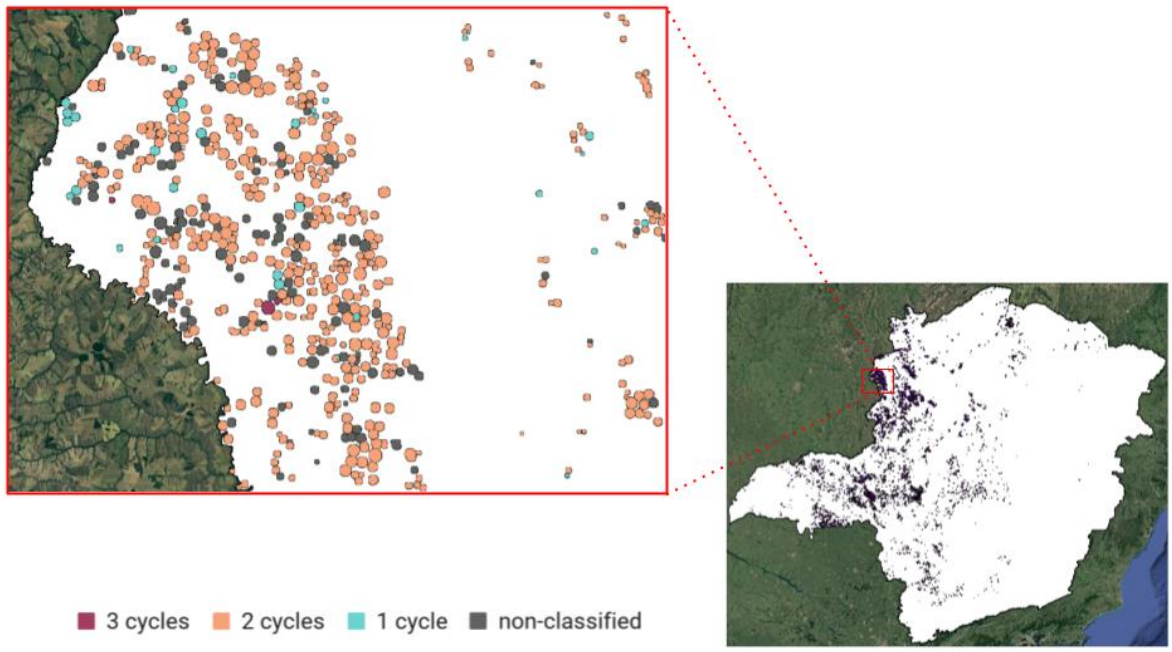

Figure 30: Example of center pivot irrigation mapped with one, two and three cycles in Minas Gerais state.

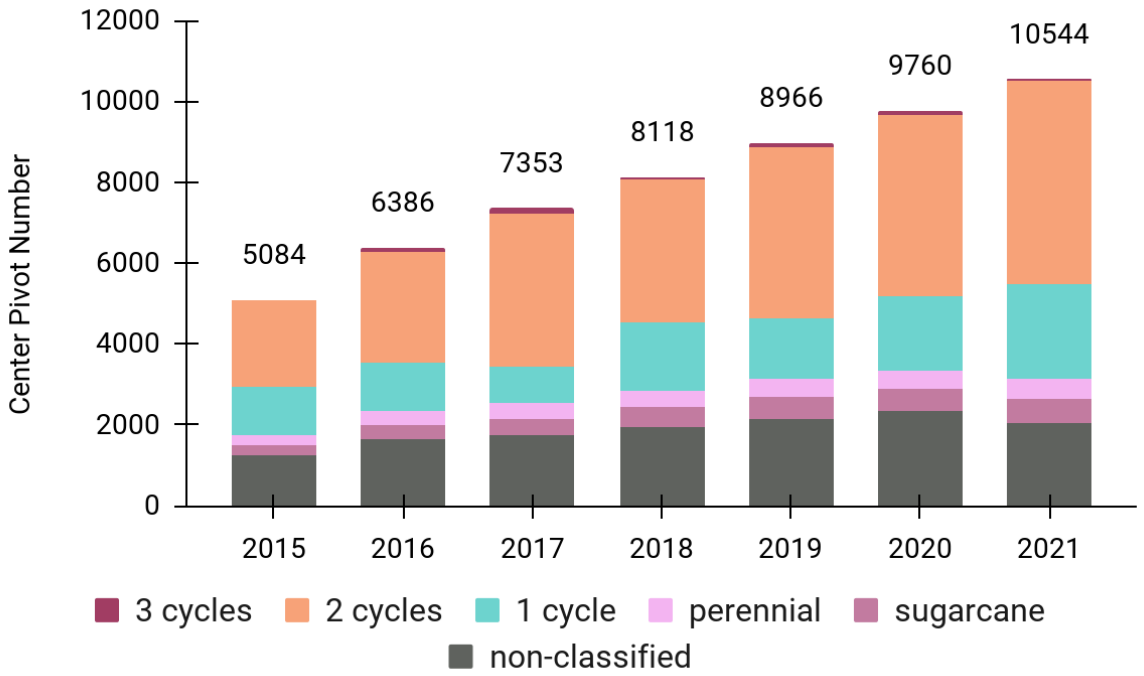

Figure 31: Number of center pivot irrigation with one, two and three cycles, perennial, sugarcane and non-classified in Minas Gerais state.

Overall, for Minas Gerais state, 19% of center pivot irrigation has one crop cycle, while 46% present two crop cycles, and approximately 1% were cultivated three times over the analyzed years (2015-2021). In addition, approximately 24% of center pivot irrigation was not classified as a function of methodology limitation. Around 6% of these pivots were identified as perennial pivots and 5% as sugarcane.

In addition to this information, through the results, some general information about the region's crop dynamic was summarized. It was possible to identify the months of start and end cycle, the amount of days of each cycle and how much precipitation occurred in this period, also to each cycle. Figure 32 presents a temporal synthesis (2015-2021) of this information for the pivots identified with crop dynamics (pivots with 1, 2 or 3 cycles), in the Minas Gerais state.

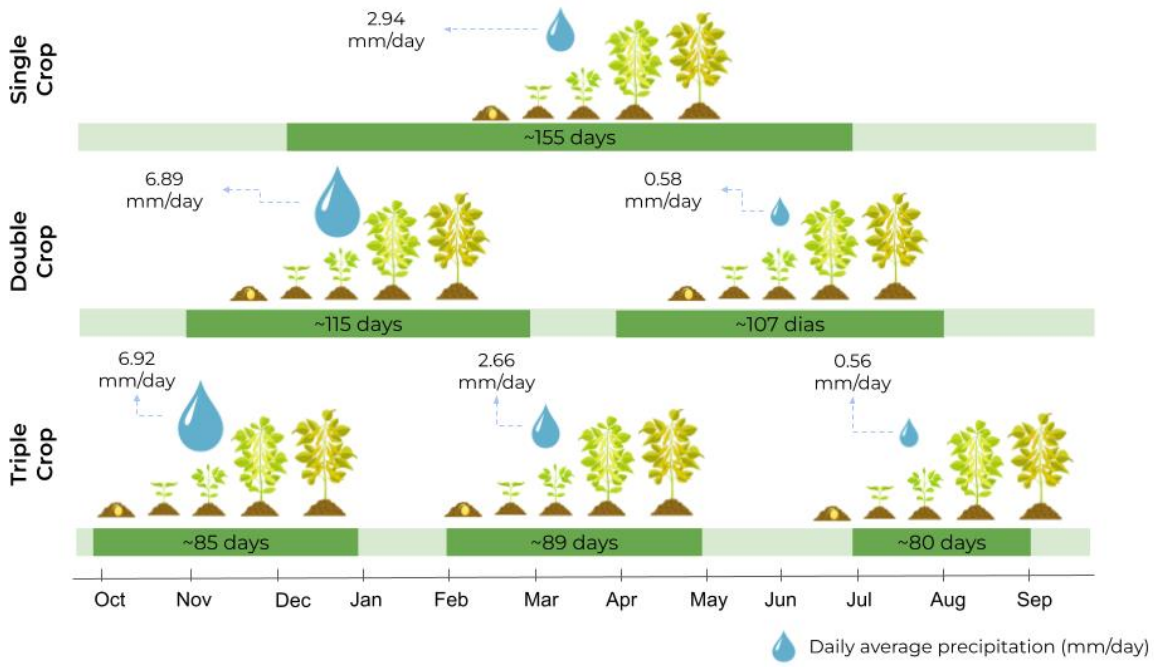

Figure 32: Summary of pivot dynamics for Minas Gerais state between 2015 and 2021.

In Figure 32 presented above, it is possible to see that both the start and end months of each cycle, as well as its duration and daily average precipitation varies according to the amount of times the pivots have been cultivated in the year.

For instance, on pivots with one single crop cycle, the cultivation usually starts in December with a harvest occurring around July. Pivots with only one cycle present a longer cycle duration, of approximately 155 days,. The daily precipitation is about 2.94 mm/day, since the cycle also extends over rainy (December, November, January and February, June and July) and dry (May, June and July) months in this region.

For pivots that present a double-crop there is a different dynamic. In these pivots the cycle duration is around 115 days for the first cycle and around 107 days for the second cycle. Comparing pivots with single and double-crops it is possible to verify that for double-crop pivots the period when the cultivation occurred was usually earlier than the single-crop pivots, with planting starting around November and harvesting around March. As this first cycle of the double crop pivots is concentrated in the rainiest months of this region, the daily average precipitation is higher, around 6.89 mm/day. Regarding the second cycle of double-crop pivots, this usually starts planting around April and harvesting usually occurs in August. Because it comprises mainly the winter months, this period presents low precipitation, with a rate of approximately 0.58 mm/day, indicating that only the precipitation of the period is not sufficient for the development of the crop, requiring the use of an irrigation system for this second harvest.

For pivots with triple-crop the crop duration is even shorter than pivots with one or double-crops. In these pivots with triple-crops, generally the cycles extend from from 80 to 89 days. In addition, the period of cultivation of the first cycle starts earlier than pivots with single or double-crops, starting in October and the harvest occurring in January. The second cycle normally starts in February and the harvest occurs in May, while the third cycle extends from July to September. The

first two cycles of triple-crop pivots take place at least partially in the region's rainy season,, with a rate about 6.92 mm/day for the first cycle and 2.66 mm/day for the second cycle, indicating a lower dependency of the irrigation system in the first cycle compared to the second one. However, during the third cycle precipitation rate is about 0.56 mm/day, suggesting a significant increase of irrigation importance for crop development.

5 References

Abatzoglou, J. T., Dobrowski, S. Z., Parks, S. A., & Hegewisch, K. C. (2018). TerraClimate, a high-resolution global dataset of monthly climate and climatic water balance from 1958–2015. *Scientific data*, *5*(1), 1-12.

AGÊNCIA NACIONAL DE ÁGUAS (ANA). Atlas irrigação: uso da água na agricultura irrigada /Agência Nacional de Águas. Brasília: ANA, 2017.

AGÊNCIA NACIONAL DE ÁGUAS (ANA). Levantamento da agricultura irrigada por pivôs centrais no Brasil/Agência Nacional de Águas, Embrapa Milho e Sorgo. 2. ed. Brasília: ANA, 2019a.

AGÊNCIA NACIONAL DE ÁGUAS (ANA). Levantamento da cana-de-açúcar irrigada e fertirrigada no Brasil/Agência Nacional de Águas. 2. ed. Brasília: ANA, 2019b.

AGÊNCIA NACIONAL DE ÁGUAS (ANA). Polos nacionais de agricultura irrigada: mapeamento de áreas irrigadas com imagens de satélite/Agência Nacional de Águas - Brasília: ANA, 2020.

AGÊNCIA NACIONAL DE ÁGUAS (ANA). Atlas irrigação: uso da água na agricultura irrigada (2ª edição)/Agência Nacional de Águas - Brasília: ANA, 2021a.

AGÊNCIA NACIONAL DE ÁGUAS (ANA). Mapeamento do arroz irrigado no Brasil/Agência Nacional de Águas, Companhia Nacional de Abastecimento. Brasília: ANA, 2021b.

Breiman, Leo. Random forests. Machine learning, v. 45, n. 1, p. 5-32, 2001.

EMPRESA BRASILEIRA DE PESQUISA E AGROPECUÁRIA (EMBRAPA). Dados conjunturais da produção de arroz (Oryza sativa L.) no Brasil (1986 a 2019): área, produção e rendimento. Santo Antônio de Goiás: Embrapa Arroz e Feijão, 2020. Available at: <http://www.cnpaf.embrapa.br/socioeconomia/index.htm>. Access on : 07/04/2022.

INSTITUTO BRASILEIRO DE GEOGRAFIA E ESTATÍSTICA (IBGE). 2009. Censo agropecuário 2006: resultados definitivos. Rio de Janeiro: IBGE, 2009.

INSTITUTO BRASILEIRO DE GEOGRAFIA E ESTATÍSTICA (IBGE). 2019. Censo agropecuário 2017: resultados definitivos. Rio de Janeiro: IBGE, 2019.

Deines, J. M., Kendall, A. D., Crowley, M. A., Rapp, J., Cardille, J. A., & Hyndman, D. W. (2019). Mapping three decades of annual irrigation across the US High Plains Aquifer using Landsat and Google Earth Engine. Remote Sensing of Environment, *233*, 111400.

Farr, T.G., Rosen, P.A., Caro, E., Crippen, R., Duren, R., Hensley, S., Kobrick, M., Paller, M., Rodriguez, E., Roth, L., Seal, D., Shaffer, S., Shimada, J., Umland, J., Werner, M., Oskin, M., BURBANK, D., and Alsdorf, D.E. (2007). The shuttle radar topography mission: Reviews of Geophysics, v. 45, no. 2, RG2004, at <https://doi.org/10.1029/2005RG000183>.

Funk, C., Peterson, P., Landsfeld, M., Pedreros, D., Verdin, J., Shukla, S., ... & Michaelsen, J. (2015). The climate hazards infrared precipitation with stations—a new environmental record for monitoring extremes. *Scientific data*, *2*(1), 1-21.

Gao, B. C. (1996). NDWI—A normalized difference water index for remote sensing of vegetation liquid water from space. *Remote sensing of environment*, *58*(3), 257-266.

Jaccard, P. (1901). Étude comparative de la distribution florale dans une portion des Alpes et des Jura. *Bull Soc Vaudoise Sci Nat*, *37*, 547-579.

Jiang, Z., Huete, A. R., Didan, K., & Miura, T. (2008). Development of a two-band enhanced vegetation index without a blue band. *Remote sensing of Environment*, *112*(10), 3833-3845.

Jönsson, P., & Eklundh, L. (2004). TIMESAT—a program for analyzing time-series of satellite sensor data. *Computers & geosciences*, *30*(8), 833-845.

Nagler, P. L., Inoue, Y., Glenn, E. P., Russ, A. L., & Daughtry, C. S. T. (2003). Cellulose absorption index (CAI) to quantify mixed soil–plant litter scenes. Remote Sensing of Environment, 87(2-3), 310-325.

Ronneberger, O.; Fischer, P.; Brox, T. (2015). U-Net: Convolutional networks for biomedical image segmentation. In International Conference on Medical Image Computing and Computer-Assisted Intervention; Springer: Berlin, Germany, 2015; pp. 234–241.

Rouse, J., Haas, R., Schell, J., & Deering, D. (1974). Monitoring vegetation systems in the great plains with ERTS. In *Proceedings of the Third Earth Resources Technology Satellite—1 Symposium; NASA SP-351* (pp. 309-317).

Saraiva, M., Protas, É., Salgado, M., & Souza Jr, C. (2020). Automatic Mapping of Center Pivot Irrigation Systems from Satellite Images Using Deep Learning. Remote Sensing, 12(3), 558.

Whittaker, E. T. (1922). On a new method of graduation. *Proceedings of the Edinburgh Mathematical Society*, *41*, 63-75.